ISSN 2310-6697
otoiser—open transactions on independent scientific-engineering research

FUNKTECHNIKPLUS # JOURNAL

Théorie—Expérimentation—Métrologie—Logiciel—Applications

ISSUE 2 — SUNDAY 17 NOVEMBER 2013 — YEAR 1

This European Journal defends
honesty in science and ethics in engineering

Publisher — **otoiser** open transactions on independent scientific-engineering research — **ARG NP UoP** Antennas Research Group Non Profit Union of Persons — Hauptstraße 52, 2831 Scheiblingkirchen, Austria — **www.otoiser.org** — **www.antennas.gr**

Language — We declare the origins of the Journal by using English, German and French, as well as, a Hellenic vignette, in the cover page. However, since we recognize the dominance of USA English in technical literature, we adopted it as the Journal's language, although it is not our native language.

Focus — We consider Radio—FUNK, which still creates a vivid impression of the untouchable, and its Technology—TECHNIK, from an Advanced—PLUS point of view. That is, we dynamically focus at any scientific-engineering discipline producing FUNKTECHNIKPLUS Théorie, Expérimentation, Métrologie, Logiciel, ou Applications.

Scope — We emphasize this scope broadness by extending the title of the Journal with a Doppelkreuz-Zeichen #, which we use as a placeholder for the disciplines of Editorial Board: # Electrical — # Electronics — # Computer — # Telecommunications — Engineering # Computer Science # Applied Mathematics, etc.

Frequency — We regularly publish 3 issues per year on January, May, and September as well as an issue every 3 papers.

Editions — We follow the arXiv.org system, that is the 1st edition date of every issue is on the cover page and any update date is on the odd pages with its version on all pages.

Format — We use the uncommon for Journals A5 paper size and the much readable Liberation Mono fixed-space font, with hyphenation, justification, and unfixed word spacing, to display 2 pages side-by-side on widescreen monitors with WYSIWYG printout. We can consider only papers in ODF odt or MS doc format written in LibreOffice or MS Office with MathType. We use PDFCreator and PDF—Xchange to produce pdf and export to images for printing on demand and electronic publishing.

License — We use the free Open Journal System OJS from the PKP Public Knowledge Project for internet publication

Please download the latest *About* edition from
about.ftpj.otoiser.org

Editorial Board

Technical Support

Information for Peers
Guiding Principles

This is a small, but independent, low profile Journal, in which we are all — Authors — Reviewers — Readers — Editors — free at last to be Peers in Knowledge, without suffering from either:

— Journal roles or positions,

— Professional, amateur, or academic statuses, or

— Established impact factorizations,

but with the following Guiding Principles:

Authors — We do know what work means; and we do respect the research work of the scientist — engineer; and we do want to highlight this work; and we do decided to found this Journal; and we do publish this work openly; and furthermore, we do care for the work of the technical author, especially the beginner one, whom we do support strongly as follows:

1 We encourage the author to submit his own paper written just in Basic English plus Technical Terminology.

2 We encourage the author even to select a pen name, which may drop it at any time to reveal his identity.

3 We encourage the author to submit an accepted for publication paper, which he was forced to decline that publication because it would be based on a review with unacceptable evaluation or comments.

4 We encourage the author to resubmit a non accepted for publication paper that was rejected after a poor, inadequate, unreasonable, irresponsible, incompetent, or ticking only, review.

5 We encourage the author to submit a paper that he already self-archived on some open repository, such as arXiv.org.

6 We encourage the author to self-archive all of the preprint and postprint versions of his paper.

7 We provide the author with a decent, express review process of up to just 4 weeks, by at least 2 peers, never have been co-authors with him.

8 We provide the author with a selection of review process between: a traditional, anonymous, peer review decision, and an immediate online pre-publication of his paper followed by an open discussion with at least 2 reviewers.

9 We immediately accept for publication a research paper directly resulting from a Project Report, Diploma-, Master-, or PhD-thesis, which the author already has successfully defended before a committee of experts and he can mention 2 members of it, who reviewed and approved his work.

10 We immediately publish online a paper, as soon as, it is accepted for publication in the Journal.

11 We quickly print-on-demand an issue every 3 papers, in excess of the 3 issues we regularly publish 3 times a year.

12 We do not demand from the author to transfer his own copyright to us.

13 Nevertheless, we publish only an original research work paper and only if the author does assure us that he owns the copyright of his own paper and submit this paper or a revised version of it to the Journal for publication or even for republication under the Creative Commons—Attribution 3.0 Unported License, CC-BY 3.

Reviewers — Any peer may voluntarily becomes a reviewer of the Journal in his expertize for as long as he wishes. Each author of the Journal has to support the peer-to-peer review process by reviewing one paper, written by non co-author(s) of him, for every one of his papers published in the Journal.

Readers — Any reader is a potential reviewer. We welcome online comments and post-reviews by the readers.

Editors — Any editor holds a PhD degree, to objectively prove that he really has the working experience of passing through the established publishing system. An editor pre-reviews a paper in order to check its compliance to the Guiding Principles and to select the appropriate reviewers of the Journal. We can only accept for consideration papers in the expertise areas currently shown in the Editorial Board page. However, since we are willing to amplify and extend the Scope of the Journal, we welcome the volunteer expert, in any subject included into it, who wants to join the Board, if he unreservedly accepts our Guiding Principles.

Antennas Research Group — Non-Profit 12(3) * Union of Persons

* The Constitution of Greece, Article: 12(3) 2008: www.hellenicparliament.gr/en/Vouli—ton—Ellinon/To—Politevma
* The Hellenic Supreme Court of Civil and Penal Law: www.areiospagos.gr/en/ — Court Rulings:Civil|A1|511|2008

Submissions
sub@ftpj.otoiser.org

Electronic Publishing
www.ftpj.otoiser.org

Printing-on-Demand
pod@ftpj.otoiser.org
Directly:
Georgios Tontrias, msn.expresscopy.xan@hotmail.com
ExpressCopy, V.Sofias 8, 671 00, Xanthi, Greece

More — Detailed information will be available soon at:
www.ftpj.otoiser.org/gp

Direct and Related Far-Field Inverse Scattering Problems for Spherical Electromagnetic Waves in Chiral Media

N.M. Berketis *

Independent Researcher, Athens, Greece

Abstract

This paper studies the direct and inverse scattering problem when the incident electromagnetic field is a time harmonic point – generated wave in a chiral media and the scatterer is a perfectly conducting sphere. The exact Green's function and the electric far-field patterns of the scattering problem are constructed. For a small sphere, a closed-form approximation of the scattered wave field at the source of the incident spherical wave is obtained. Also treats the same inverse problem using far-field results via the leading order term in the low-frequency asymptotic expansion of the scattering cross-section.

Introduction

In a homogeneous isotropic chiral media the electromagnetic fields are composed of left – circularly polarized (LCP) and right – circularly polarized (RCP) components, which have different wave numbers and independent directions of propagation.

The LCP and RCP components are assumed to be spherical Beltrami fields since in practice such wave fields are more readily realized.

In this work, the author has studied the electromagnetic waves in chiral media produced by a point source in the vicinity of the scatterer. In particular, in [1], [2], reciprocity, optical and general scattering theorems for stimulation of point-source asymmetric media have been demonstrated. This paper studies the inverse problem of far field [2]. Specifically, we measure the scattering cross-section for a five-point source area.

In the second Section, considering Bohren decomposition into suitable Beltrami fields, we formulate the direct scattering problem of a spherical electromagnetic wave by a perfectly conducting obstacle. This problem is well posed, the existence and

uniqueness has been proved in [1], [3].

In the third Section, after expanding the incident field in terms of spherical wave functions, we obtain the exact solution of the scattering problem as well as an expansion for the electric far-field pattern [2].

Finally in the fourth Section, we consider either LCP or RCP incidence and we obtain an approximation of the scattering cross-section. For the far-field experiments, we measure the scattering cross-section for various point source locations [2].

Statement of the problem

Our goal is to study the direct and inverse scattering problems when the incident electromagnetic field is a time harmonic point – generated wave in a chiral medium and the scatterer is a perfectly conducting sphere of radius a centered at the origin. The exterior space $(r = |\mathbf{r}| > a)$ is an infinite homogeneous isotropic chiral medium with chirality measure β, electric permittivity ε and magnetic permeability μ.

We consider a time harmonic spherical electromagnetic wave due to a point source at P_0 with position vector $\mathbf{r}_0$ with respect to an origin O in the vicinity of the scatterer. In order to define spherical electromagnetic fields $\mathbf{E}_{\mathbf{r}_0}$, $\mathbf{H}_{\mathbf{r}_0}$, we make use of the Bohren decomposition into Beltrami fields $\mathbf{Q}_{L,\mathbf{r}_0}$ and $\mathbf{Q}_{R,\mathbf{r}_0}$, as follows

$$\begin{aligned} \mathbf{E}_{\mathbf{r}_0} &= \mathbf{Q}_{L,\mathbf{r}_0} + \mathbf{Q}_{R,\mathbf{r}_0} \\ \mathbf{H}_{\mathbf{r}_0} &= \frac{1}{i\eta}\left(\mathbf{Q}_{L,\mathbf{r}_0} - \mathbf{Q}_{R,\mathbf{r}_0}\right) \end{aligned} \tag{1}$$

Where $\eta = (\mu/\varepsilon)^{1/2}$ is the intrinsic impedance of the chiral medium. The Beltrami fields satisfy the equations [4], [5],

$$\begin{aligned} \nabla\times\mathbf{Q}_{L,\mathbf{r}_0} &= \gamma_L\mathbf{Q}_{L,\mathbf{r}_0} \\ \nabla\times\mathbf{Q}_{R,\mathbf{r}_0} &= -\gamma_R\mathbf{Q}_{L,\mathbf{r}_0} \end{aligned} \tag{2}$$

where γ_L and γ_R are wave numbers given by,

$$\gamma_L = \frac{k}{1-k\beta},\ \gamma_R = \frac{k}{1+k\beta} \tag{3}$$

with $k = \omega(\varepsilon\mu)^{1/2}$, ω being the angular frequency. The indices L and R denote the LCP and RCP fields respectively. The spherical incident Beltrami fields with suitable normalization have the form [1], [2],

$$\mathbf{Q}^{inc}_{L,\mathbf{r}_0}(\mathbf{r}\,|\,\hat{\mathbf{p}}_L) = \frac{1}{2}\,(\tilde{\mathbf{I}} + \frac{1}{\gamma_L^2}\nabla\nabla + \frac{1}{\gamma_L}\,\nabla\times\tilde{\mathbf{I}})\,(\frac{h_0(\gamma_L|\mathbf{r}-\mathbf{r}_0|)}{h_0(\gamma_L r_0)})\cdot\hat{\mathbf{p}}_L = \\ = \frac{2\pi r_0 e^{-i\gamma_L r_0}}{\gamma_L}\,[\gamma_L\tilde{\mathbf{G}}_{fs}(\mathbf{r},\mathbf{r}_0) + \nabla\times\tilde{\mathbf{G}}_{fs}(\mathbf{r},\mathbf{r}_0)\,]\cdot\hat{\mathbf{p}}_L \tag{4}$$

$$\mathbf{Q}^{inc}_{R,\mathbf{r}_0}(\mathbf{r}\,|\,\hat{\mathbf{p}}_R) = \frac{1}{2}\,(\tilde{\mathbf{I}} + \frac{1}{\gamma_R^2}\nabla\nabla - \frac{1}{\gamma_R}\,\nabla\times\tilde{\mathbf{I}})\,(\frac{h_0(\gamma_R|\mathbf{r}-\mathbf{r}_0|)}{h_0(\gamma_R r_0)})\cdot\hat{\mathbf{p}}_R = \\ = \frac{2\pi r_0 e^{-i\gamma_R r_0}}{\gamma_R}\,[\gamma_R\tilde{\mathbf{G}}_{fs}(\mathbf{r},\mathbf{r}_0) - \nabla\times\tilde{\mathbf{G}}_{fs}(\mathbf{r},\mathbf{r}_0)\,]\cdot\hat{\mathbf{p}}_R \tag{5}$$

where $h_0(x) = h_0^1(x) = e^{ix}/(ix)$ is the zeroth-order spherical Hankel function of first kind, $\tilde{\mathbf{I}} = \hat{\mathbf{x}}\hat{\mathbf{x}} + \hat{\boldsymbol{\psi}}\hat{\boldsymbol{\psi}} + \hat{\mathbf{z}}\hat{\mathbf{z}}$ is the identity dyadic, $r_0 = |\mathbf{r}_0|$ and $\tilde{\mathbf{G}}_{fs}(\mathbf{r},\mathbf{r}_0)$ is the free space dyadic Green function [4]. The constant unit vectors $\hat{\mathbf{p}}_L$ and $\hat{\mathbf{p}}_R$ satisfy the relations

$$\hat{\mathbf{r}}_0\cdot\hat{\mathbf{p}}_L = \hat{\mathbf{r}}_0\cdot\hat{\mathbf{p}}_R = 0 \\ \hat{\mathbf{r}}_0\times\hat{\mathbf{p}}_L = i\hat{\mathbf{p}}_L \\ \hat{\mathbf{r}}_0\times\hat{\mathbf{p}}_R = -i\hat{\mathbf{p}}_R \tag{6}$$

We note that when $r_0\to\infty$, the incident electric field

$$\mathbf{E}^{inc}_{\mathbf{r}_0}(\mathbf{r}\,|\,\hat{\mathbf{p}}_L,\hat{\mathbf{p}}_R) = \\ = \mathbf{Q}^{inc}_{L,\mathbf{r}_0}(\mathbf{r}\,|\,\hat{\mathbf{p}}_L) + \mathbf{Q}^{inc}_{R,\mathbf{r}_0}(\mathbf{r}\,|\,\hat{\mathbf{p}}_R) \tag{7}$$

reduces to plane electric wave with direction of propagation $-\hat{\mathbf{r}}_0$ and polarizations $\hat{\mathbf{p}}_L$, $\hat{\mathbf{p}}_R$, since

$$\lim_{r_0\to\infty}\mathbf{Q}^{inc}_{L,\mathbf{r}_0}(\mathbf{r}\,|\,\hat{\mathbf{p}}_L) = e^{-i\gamma_L\hat{\mathbf{r}}_0\cdot\mathbf{r}}\hat{\mathbf{p}}_L = \\ = \mathbf{Q}^{inc}_{L}(\mathbf{r};-\hat{\mathbf{r}}_0,\hat{\mathbf{p}}_L) \tag{8}$$

$$\lim_{r_0\to\infty}\mathbf{Q}^{inc}_{R,\mathbf{r}_0}(\mathbf{r}\,|\,\hat{\mathbf{p}}_R) = e^{-i\gamma_R\hat{\mathbf{r}}_0\cdot\mathbf{r}}\hat{\mathbf{p}}_R = \\ = \mathbf{Q}^{inc}_{R}(\mathbf{r};-\hat{\mathbf{r}}_0,\hat{\mathbf{p}}_R) \tag{9}$$

We consider $\mathbf{E}^{inc}_{\mathbf{r}_0}$ is incident upon a perfectly conducting sphere of radius a. Then, we want to calculate the scattered electric field $\mathbf{E}^{sc}_{\mathbf{r}_0}$, which is the unique solution of the following exterior boundary value problem

$$\nabla\times\nabla\times\mathbf{E}^{sc}_{\mathbf{r}_0}(\mathbf{r}) - 2\gamma^2\beta\nabla\times\mathbf{E}^{sc}_{\mathbf{r}_0}(\mathbf{r}) - \gamma^2\mathbf{E}^{sc}_{\mathbf{r}_0}(\mathbf{r}) = \mathbf{0},\ r > a \tag{10}$$

$$\hat{\mathbf{n}}\times\mathbf{E}^{sc}_{\mathbf{r}_0}(\mathbf{r}) = -\,\hat{\mathbf{n}}\times\mathbf{E}^{inc}_{\mathbf{r}_0}(\mathbf{r}),\ r = a \tag{11}$$

The Silver-Müller radiation condition is modified as follows

$$\hat{\mathbf{r}}\times\nabla\times\mathbf{E}^{sc}_{\mathbf{r}_0}(\mathbf{r}) - \beta\gamma^2\hat{\mathbf{r}}\times\mathbf{E}^{sc}_{\mathbf{r}_0}(\mathbf{r}) + \frac{\mathrm{i}\gamma^2}{k}\mathbf{E}^{sc}_{\mathbf{r}_0}(\mathbf{r}) = o(\frac{1}{r}),\ r\to\infty \tag{12}$$

uniformly in all directions $\hat{\mathbf{r}}\in S^2$, where S^2 is the unit sphere in $\mathbb{R}^3$, $\hat{\mathbf{n}}$ is the outward normal unit vector on the scatterer and $\gamma^2 = \gamma_L\gamma_R$. The scattered electric field will be depended on the polarizations $\hat{\mathbf{p}}_L$, $\hat{\mathbf{p}}_R$ and will have the decomposition

$$\mathbf{E}^{sc}_{\mathbf{r}_0}(\mathbf{r}\,|\,\hat{\mathbf{p}}_L,\hat{\mathbf{p}}_R) = \mathbf{Q}^{sc}_{L,\mathbf{r}_0}(\mathbf{r}\,|\,\hat{\mathbf{p}}_L,\hat{\mathbf{p}}_R) + \mathbf{Q}^{sc}_{R,\mathbf{r}_0}(\mathbf{r}\,|\,\hat{\mathbf{p}}_L,\hat{\mathbf{p}}_R) \tag{13}$$

where $\mathbf{Q}^{sc}_{L,\mathbf{r}_0}(\mathbf{r}\,|\,\hat{\mathbf{p}}_L,\hat{\mathbf{p}}_R)$ and $\mathbf{Q}^{sc}_{R,\mathbf{r}_0}(\mathbf{r}\,|\,\hat{\mathbf{p}}_L,\hat{\mathbf{p}}_R)$ are the corresponding scattered Beltrami fields which have the following behavior, when $r\to\infty$

$$\mathbf{Q}^{sc}_{L,\mathbf{r}_0}(\mathbf{r}\,|\,\hat{\mathbf{p}}_L,\hat{\mathbf{p}}_R) = h_0(\gamma_L r)\cdot \cdot\mathbf{g}_{L,\mathbf{r}_0}(\hat{\mathbf{r}}\,|\,\hat{\mathbf{p}}_L,\hat{\mathbf{p}}_R) + O(\frac{1}{r^2}) \tag{14}$$

$$\mathbf{Q}^{sc}_{R,\mathbf{r}_0}(\mathbf{r}\,|\,\hat{\mathbf{p}}_L,\hat{\mathbf{p}}_R) = h_0(\gamma_R r)\cdot \cdot\mathbf{g}_{R,\mathbf{r}_0}(\hat{\mathbf{r}}\,|\,\hat{\mathbf{p}}_L,\hat{\mathbf{p}}_R) + O(\frac{1}{r^2}) \tag{15}$$

The functions $\mathbf{g}_{L,\mathbf{r}_0}$ and $\mathbf{g}_{R,\mathbf{r}_0}$ are the LCP and RCP far–field patterns respectively [4], [6].

If either a LCP or a RCP spherical electric wave $\mathbf{E}^{inc}_{\mathbf{r}_0}(\mathbf{r}\,|\,\hat{\mathbf{p}}_A)$, $A = L, R$, is incident upon the scatterer, then the scattering cross–section, is given by [6],

$$\sigma^{sc}_{A,\mathbf{r}_0} = \int_{S^2}[\frac{1}{\gamma_L^2}\left|\mathbf{g}_{L,\mathbf{r}_0}(\hat{\mathbf{r}}\,|\,\hat{\mathbf{p}}_A)\right|^2 + \frac{1}{\gamma_R^2}\left|\mathbf{g}_{R,\mathbf{r}_0}(\hat{\mathbf{r}}\,|\,\hat{\mathbf{p}}_A)\right|^2]\,ds(\hat{\mathbf{r}}) \tag{16}$$

Exact Green's function

We take spherical coordinates (r,θ,φ) where $\theta\in[0,\pi]$ and $\varphi\in[0,2\pi)$, with the origin at the center of the spherical scatterer, so that the point source is at $r = r_0$, $\theta = 0$.

Thus, $\mathbf{r}_0 = r_0\hat{\mathbf{z}}$, $\hat{\mathbf{p}}_L = \frac{1}{\sqrt{2}}(\hat{\mathbf{x}} - \mathrm{i}\hat{\boldsymbol{\psi}})$ and $\hat{\mathbf{p}}_R = \frac{1}{\sqrt{2}}(\hat{\mathbf{x}} + \mathrm{i}\hat{\boldsymbol{\psi}})$, where $\hat{\mathbf{x}}, \hat{\boldsymbol{\psi}}$ and $\hat{\mathbf{z}}$ are unit vectors in

the x, ψ and z directions, respectively. Using spherical vector wave functions, [4], [5], [7], and taking into account (4), and (5), we obtain [2],

$$\mathbf{Q}^{inc}_{L,\mathbf{r}_0}(\mathbf{r} \mid \hat{\mathbf{p}}_L) = \sum_{n=1}^{\infty} B_n^L \{\mathbf{L}^{(1)}_{o1n}(\gamma_L \mathbf{r}) + \mathrm{i}\mathbf{L}^{(1)}_{e1n}(\gamma_L \mathbf{r})\} \tag{17}$$

or

$$\mathbf{Q}^{inc}_{R,\mathbf{r}_0}(\mathbf{r} \mid \hat{\mathbf{p}}_R) = \sum_{n=1}^{\infty} B_n^R \{\mathbf{R}^{(1)}_{o1n}(\gamma_R \mathbf{r}) - \mathrm{i}\mathbf{R}^{(1)}_{e1n}(\gamma_R \mathbf{r})\} \tag{18}$$

where, for $r < r_0$

$$B_n^A = \frac{1}{2\sqrt{2} h_0(\gamma_A r_0)} \frac{2n+1}{n(n+1)} H_n(\gamma_A r_0)$$

and (19)

$$H_n(\gamma_A r_0) = h_n(\gamma_A r_0) - \mathrm{i}\tilde{h}_n(\gamma_A r_0)$$

with $A = L, R$. The h_n is a spherical Hankel function of first kind of order n,

$$\tilde{h}(x) = x^{-1} h_n(x) + h_n'(x),$$

$\mathbf{L}^{(\rho)}_{s1n}$ and $\mathbf{R}^{(\rho)}_{s1n}$, with $s = e$, or o (even or odd) are the spherical functions [4], [5],

$$\begin{aligned} \mathbf{L}^{(\rho)}_{s1n}(\gamma_L \mathbf{r}) &= \mathbf{M}^{(\rho)}_{s1n}(\gamma_L \mathbf{r}) + \mathbf{N}^{(\rho)}_{s1n}(\gamma_L \mathbf{r}) \\ \mathbf{R}^{(\rho)}_{s1n}(\gamma_R \mathbf{r}) &= \mathbf{M}^{(\rho)}_{s1n}(\gamma_R \mathbf{r}) - \mathbf{N}^{(\rho)}_{s1n}(\gamma_R \mathbf{r}) \end{aligned} \tag{20}$$

where $\rho = 1, 3$, the $\mathbf{M}^{(\rho)}_{s1n}$ and $\mathbf{N}^{(\rho)}_{s1n}$ are known spherical vector function [7]. The scattered electric field that comes from a LCP incident field or a RCP incident field has a similar expansion to (17) or to (18)

$$\begin{aligned} \mathbf{E}^{sc}_{\mathbf{r}_0}(\mathbf{r} \mid \hat{\mathbf{p}}_L) &= \mathbf{Q}^{sc}_{L,\mathbf{r}_0}(\mathbf{r} \mid \hat{\mathbf{p}}_L) + \mathbf{Q}^{sc}_{R,\mathbf{r}_0}(\mathbf{r} \mid \hat{\mathbf{p}}_L) = \\ &= \sum_{n=1}^{\infty} B_n^L a_n^L \{\mathbf{L}^{(3)}_{o1n}(\gamma_L \mathbf{r}) + \mathrm{i}\mathbf{L}^{(3)}_{e1n}(\gamma_L \mathbf{r})\} + \sum_{n=1}^{\infty} B_n^L a_n^R \{\mathbf{R}^{(3)}_{o1n}(\gamma_R \mathbf{r}) + \mathrm{i}\mathbf{R}^{(3)}_{e1n}(\gamma_R \mathbf{r})\} \end{aligned} \tag{21}$$

or

$$\begin{aligned} \mathbf{E}^{sc}_{\mathbf{r}_0}(\mathbf{r} \mid \hat{\mathbf{p}}_R) &= \mathbf{Q}^{sc}_{L,\mathbf{r}_0}(\mathbf{r} \mid \hat{\mathbf{p}}_R) + \mathbf{Q}^{sc}_{R,\mathbf{r}_0}(\mathbf{r} \mid \hat{\mathbf{p}}_R) + \\ &= \sum_{n=1}^{\infty} B_n^R b_n^L \{\mathbf{L}^{(3)}_{o1n}(\gamma_L \mathbf{r}) - i\mathbf{L}^{(3)}_{e1n}(\gamma_L \mathbf{r})\} + \sum_{n=1}^{\infty} B_n^R b_n^R \{\mathbf{R}^{(3)}_{o1n}(\gamma_R \mathbf{r}) - \mathrm{i}\mathbf{R}^{(3)}_{e1n}(\gamma_R \mathbf{r})\} \end{aligned} \tag{22}$$

Using the boundary condition (11) on $r = a$, we obtain [2],

$$a_n^L = -\frac{j_n(\gamma_L a)\,\tilde{h}_n(\gamma_R a) + \tilde{j}_n(\gamma_L a)\,h_n(\gamma_R a)}{h_n(\gamma_L a)\,\tilde{h}_n(\gamma_R a) + \tilde{h}_n(\gamma_L a)\,h_n(\gamma_R a)} \tag{23}$$

and

$$a_n^R = -\frac{j_n(\gamma_L a)\,\tilde{h}_n(\gamma_L a) - \tilde{j}_n(\gamma_L a)\,h_n(\gamma_L a)}{h_n(\gamma_L a)\,\tilde{h}_n(\gamma_R a) + \tilde{h}_n(\gamma_L a)\,h_n(\gamma_R a)} \tag{24}$$

or

$$b_n^L = -\frac{j_n(\gamma_R a)\,\tilde{h}_n(\gamma_R a) - \tilde{j}_n(\gamma_R a)\,h_n(\gamma_R a)}{h_n(\gamma_L a)\,\tilde{h}_n(\gamma_R a) + \tilde{h}_n(\gamma_L a)\,h_n(\gamma_R a)} \tag{25}$$

and

$$b_n^R = -\frac{j_n(\gamma_R a)\,\tilde{h}_n(\gamma_L a) + \tilde{j}_n(\gamma_R a)\,h_n(\gamma_L a)}{h_n(\gamma_L a)\,\tilde{h}_n(\gamma_R a) + \tilde{h}_n(\gamma_L a)\,h_n(\gamma_R a)} \tag{26}$$

Using the asymptotic forms [4], [7],

$$\mathbf{L}_{s1n}^{(3)}(\gamma_L \mathbf{r}) \sim \sqrt{n(n+1)}(-\mathrm{i})^n\, h_0(\gamma_L r)\,\mathbf{f}_{s1n}^L(\hat{\mathbf{r}}) \tag{27}$$

$$\mathbf{R}_{s1n}^{(3)}(\gamma_R \mathbf{r}) \sim \sqrt{n(n+1)}(-\mathrm{i})^n\, h_0(\gamma_R r)\,\mathbf{f}_{s1n}^R(\hat{\mathbf{r}}) \tag{28}$$

where let us introduce LCP Beltrami angular $\mathbf{f}_{s1n}^L(\hat{\mathbf{r}})$, and RCP Beltrami angular $\mathbf{f}_{s1n}^R(\hat{\mathbf{r}})$ [4], satisfy by relations,

$$\mathbf{f}_{s1n}^L(\hat{\mathbf{r}}) = \mathbf{C}_{s1n}(\hat{\mathbf{r}}) + \mathrm{i}\mathbf{B}_{s1n}(\hat{\mathbf{r}})\,, \quad \mathbf{f}_{s1n}^R(\hat{\mathbf{r}}) = \mathbf{C}_{s1n}(\hat{\mathbf{r}}) - \mathrm{i}\mathbf{B}_{s1n}(\hat{\mathbf{r}}) \tag{29}$$

we calculate the electric far-field patterns [2],

$$\mathbf{g}_{A,\mathbf{r}_0}^{sc}(\hat{\mathbf{r}} \mid \hat{\mathbf{p}}_L) = \sum_{n=1}^{\infty} \frac{(2n+1)(-\mathrm{i})^{n-1}}{2\sqrt{2n(n+1)}} \frac{H_n(\gamma_L r_0)}{h_0(\gamma_L r_0)} a_n^A \{\mathbf{f}_{e1n}^A(\hat{\mathbf{r}}) - \mathrm{i}\mathbf{f}_{o1n}^A(\hat{\mathbf{r}})\} \tag{30}$$

or

$$\mathbf{g}_{A,\mathbf{r}_0}^{sc}(\hat{\mathbf{r}} \mid \hat{\mathbf{p}}_R) = \sum_{n=1}^{\infty} \frac{(2n+1)(-\mathrm{i})^{n-1}}{2\sqrt{2n(n+1)}} \frac{H_n(\gamma_R r_0)}{h_0(\gamma_R r_0)} b_n^A \{-\mathbf{f}_{e1n}^A(\hat{\mathbf{r}}) - \mathrm{i}\mathbf{f}_{o1n}^A(\hat{\mathbf{r}})\} \tag{31}$$

A far-field inverse problem

So far, all of our formulas are exact. In the asymptotic results to follow, there are three parameters $\gamma_A a$, with $A = L, R$ and $\tau = a/r_0$. We note that the geometrical parameter τ must satisfy $0 < \tau < 1$ because the point source is outside of the sphere.

We assume that $|\gamma_A a| \ll 1$, as well; that is we make the so-called low-frequency assumption. From (23), (24), (26), (27), we obtain [2],

$$a_n^L \sim \frac{1+\beta k}{2\mathrm{i}\zeta_n^2(2n+1)}(\gamma_L a)^{2n+1}$$

$$a_n^R \sim -\frac{\mathrm{i}}{2n\zeta_n^2}\frac{(1-\beta k)^{n+2}}{(1+\beta k)^{n+1}}(\gamma_L a)^{2n+1}$$

$$\gamma_L a \to 0 \qquad (32)$$

or

$$b_n^L \sim -\frac{\mathrm{i}}{2n\zeta_n^2}\frac{(1+\beta k)^{n+2}}{(1-\beta k)^{n+1}}(\gamma_R a)^{2n+1}$$

$$b_n^R \sim -\frac{\mathrm{i}(1-\beta k)}{2\zeta_n^2(2n+1)}(\gamma_R a)^{2n+1}$$

$$\gamma_R a \to 0 \qquad (33)$$

where

$\zeta_n = 1\cdot 3\cdot 5\cdots(2n-1) = (2n)!/(2^n n!)$.
In particular,

$$\begin{cases} a_1^L = -\mathrm{i}\dfrac{1+\beta k}{6}(\gamma_L a)^3 + O((\gamma_L a)^5) \\ a_2^L = -\mathrm{i}\dfrac{1+\beta k}{90}(\gamma_L a)^5 + O((\gamma_L a)^7) \end{cases}$$

$$\gamma_L a \to 0 \qquad (34)$$

$$\begin{cases} a_1^R = -\dfrac{\mathrm{i}(1-\beta k)^3}{2(1+\beta k)^2}(\gamma_L a)^3 + O((\gamma_L a)^5) \\ a_2^R = -\dfrac{\mathrm{i}(1-\beta k)^4}{36(1+\beta k)^3}(\gamma_L a)^5 + O((\gamma_L a)^7) \end{cases}$$

$$\gamma_L a \to 0 \qquad (35)$$

or

$$\begin{cases} b_1^L = -\dfrac{\mathrm{i}(1+\beta k)^3}{2(1-\beta k)^2}(\gamma_R a)^3 + O((\gamma_L a)^5) \\ b_2^L = -\dfrac{\mathrm{i}(1+\beta k)^4}{36(1-\beta k)^3}(\gamma_R a)^5 + O((\gamma_L a)^7) \end{cases}$$

$$\gamma_R a \to 0 \qquad (36)$$

$$\begin{cases} b_1^R = -\dfrac{\mathrm{i}(1-\beta k)}{6}(\gamma_R a)^3 + O((\gamma_R a)^5) \\ b_2^R = -\dfrac{\mathrm{i}(1-\beta k)}{90}(\gamma_R a)^5 + O((\gamma_R a)^7) \end{cases}$$

$$\gamma_R a \to 0 \qquad (37)$$

In order to calculate $\mathbf{g}^{sc}_{A,\mathbf{r}_0}$ with an error of $O((\gamma_A a)^4)$ we only need the following [4]

$$\mathbf{C}_{o11}(\hat{\mathbf{r}}) = \frac{1}{\sqrt{2}}(\cos\varphi\,\hat{\boldsymbol{\theta}} - \cos\theta\,\sin\varphi\,\hat{\boldsymbol{\varphi}}) \qquad \mathbf{C}_{o12}(\hat{\mathbf{r}}) = (3/2)^{1/2}\cdot \cdot(\cos\theta\,\cos\varphi\,\hat{\boldsymbol{\theta}} - \cos 2\theta\,\sin\varphi\,\hat{\boldsymbol{\varphi}}) \tag{40}$$

$$\mathbf{B}_{o11}(\hat{\mathbf{r}}) = -\frac{1}{\sqrt{2}}(\cos\theta\,\sin\varphi\,\hat{\boldsymbol{\theta}} + \cos\varphi\,\hat{\boldsymbol{\varphi}}) \qquad \mathbf{B}_{e12}(\hat{\mathbf{r}}) = (3/2)^{1/2}\cdot \cdot(\cos 2\theta\,\cos\varphi\,\hat{\boldsymbol{\theta}} - \cos\theta\,\sin\varphi\,\hat{\boldsymbol{\varphi}}) \tag{41}$$

$$\mathbf{B}_{e11}(\hat{\mathbf{r}}) = \frac{1}{\sqrt{2}}(\cos\theta\,\sin\varphi\,\hat{\boldsymbol{\theta}} - \sin\varphi\,\hat{\boldsymbol{\varphi}}) \qquad \mathbf{B}_{o12}(\hat{\mathbf{r}}) = (3/2)^{1/2}\cdot \cdot(\cos 2\theta\,\sin\varphi\,\hat{\boldsymbol{\theta}} + \cos\theta\,\cos\varphi\,\hat{\boldsymbol{\varphi}}) \tag{42}$$

$$\mathbf{C}_{e11}(\hat{\mathbf{r}}) = \frac{1}{\sqrt{2}}(-\sin\varphi\,\hat{\boldsymbol{\theta}} - \cos\theta\,\cos\varphi\,\hat{\boldsymbol{\varphi}}) \qquad \hat{\mathbf{C}}_{e12}(\hat{\mathbf{r}}) = (3/2)^{1/2}\cdot \cdot(-\cos\theta\sin\varphi\,\hat{\boldsymbol{\theta}} - \cos 2\theta\cos\varphi\,\hat{\boldsymbol{\varphi}}) \tag{43}$$

So from (30) and (31), we finally obtain [2],

$$\begin{aligned}\mathbf{g}^{SC}_{A,\mathrm{r}_0}(\hat{\mathbf{r}}\,|\,\hat{\mathbf{p}}_A) = {} & \varpi_A\,\frac{(1-\varpi_A\beta k)}{8}\,[-(\gamma_A a)\tau^2[\,\mathbf{f}^A_{e11}(\hat{\mathbf{r}}) + \varpi_A \mathrm{i}\mathbf{f}^A_{o11}(\hat{\mathbf{r}})\,] + \\ & + (\gamma_A a)^2\{2\mathrm{i}\tau[\,\mathbf{f}^A_{e11}(\hat{\mathbf{r}}) + \varpi_A \mathrm{i}\mathbf{f}^A_{o11}(\hat{\mathbf{r}})\,] + \frac{\mathrm{i}}{\sqrt{3}}\,\tau^3[\,\mathbf{f}^A_{e12}(\hat{\mathbf{r}}) + \varpi_A \mathrm{i}\mathbf{f}^A_{o12}(\hat{\mathbf{r}})\,]\} + \\ & + (\gamma_A a)^3\{2[\,\mathbf{f}^A_{e11}(\hat{\mathbf{r}}) + \varpi_A \mathrm{i}\mathbf{f}^A_{o11}(\hat{\mathbf{r}})\,] + \frac{4}{3\sqrt{3}}\,\tau^2[\,\mathbf{f}^A_{e12}(\hat{\mathbf{r}}) + \varpi_A \mathrm{i}\mathbf{f}^A_{o12}(\hat{\mathbf{r}})\,]\}] + \\ & + O((\gamma_A a)^4)\end{aligned} \tag{44}$$

and

$$\begin{aligned}\mathbf{g}^{SC}_{A,\mathrm{r}_0}(\hat{\mathbf{r}}\,|\,\hat{\mathbf{p}}_{A^c}) = {} & \varpi_A\,\frac{3(1-\varpi_A\beta k)^2}{8(1+\varpi_A\beta k)}\,(\gamma_A a)\tau^2[\,\mathbf{f}^A_{e11}(\hat{\mathbf{r}}) - \varpi_A \mathrm{i}\mathbf{f}^A_{o11}(\hat{\mathbf{r}})\,] + \\ & + (\gamma_A a)^2\{-\varpi_A\,\frac{3\mathrm{i}(1-\varpi_A\beta k)}{4}\,\tau[\,\mathbf{f}^A_{e11}(\hat{\mathbf{r}}) - \varpi_A \mathrm{i}\mathbf{f}^A_{o11}(\hat{\mathbf{r}})\,] - \\ & - \varpi_A\,\frac{5\mathrm{i}}{16\sqrt{3}}\,\frac{(1-\varpi_A\beta k)^2}{1+\varpi_A\beta k}\,\tau^3[\,\mathbf{f}^A_{e12}(\hat{\mathbf{r}}) - \varpi_A \mathrm{i}\mathbf{f}^A_{o12}(\hat{\mathbf{r}})\,]\} + \\ & + (\gamma_A a)^3\{-\varpi_A\,\frac{3(1+\varpi_A\beta k)}{4}\,[\,\mathbf{f}^A_{e11}(\hat{\mathbf{r}}) - \varpi_A \mathrm{i}\mathbf{f}^A_{o11}(\hat{\mathbf{r}})\,] -\end{aligned} \tag{45}$$

$$- \varpi_A \frac{5(1-\varpi_A \beta k)}{12\sqrt{3}} \tau^2 [\mathbf{f}^A_{e12}(\hat{\mathbf{r}}) - \varpi_A \mathrm{i}\mathbf{f}^A_{o12}(\hat{\mathbf{r}})]\} + O((\gamma_A a)^4)$$

where $\varpi_A = \begin{cases} -1, A = L \\ 1, A = R \end{cases}$ and if $A = L, R$ at that case $A^c = R, L$.

Now the scattering cross-section, by LCP or RCP spherical Beltrami fields, from (16), is given by the relations [2],

$$\sigma^{sc}_{L,\mathbf{r}_0} = \int_{S^2} [\frac{1}{\gamma_L^2} \left|\mathbf{g}^{sc}_{L,\mathbf{r}_0}(\hat{\mathbf{r}} \mid \hat{\mathbf{p}}_L)\right|^2 + \frac{1}{\gamma_R^2} \left|\mathbf{g}^{sc}_{R,\mathbf{r}_0}(\hat{\mathbf{r}} \mid \hat{\mathbf{p}}_L)\right|^2] \, ds(\hat{\mathbf{r}}) =$$

$$= (\pi a^2)\{\frac{(1+\beta k)^2}{64}[\frac{16}{3}\tau^4 + (\gamma_L a)^2(\frac{64}{3}\tau^2 + 16\tau^6) + (\gamma_L a)^4(\frac{64}{3} + \frac{16}{9}\tau^4)] +$$

$$+ \frac{(1-\beta k)^4}{(1+\beta k)^2}[\frac{3}{4}\tau^4 + (\gamma_L a)^2(3\tau^2 + \frac{5(1-\beta k)^2}{16(1+\beta k)^2}\tau^6) +$$

$$+ (\gamma_L a)^4(3 + \frac{5(1-\beta k)}{9(1+\beta k)^2}\tau^4)]\} + O((\gamma_L a)^6), \ \gamma_L a \to 0 \qquad (46)$$

or

$$\sigma^{sc}_{R,\mathbf{r}_0} = \int_{S^2} [\frac{1}{\gamma_L^2} \left|\mathbf{g}^{sc}_{L,\mathbf{r}_0}(\hat{\mathbf{r}} \mid \hat{\mathbf{p}}_R)\right|^2 + \frac{1}{\gamma_R^2} \left|\mathbf{g}^{sc}_{R,\mathbf{r}_0}(\hat{\mathbf{r}} \mid \hat{\mathbf{p}}_R)\right|^2] \, ds(\hat{\mathbf{r}}) =$$

$$= (\pi a^2)\{\frac{(1-\beta k)^2}{64}[\frac{16}{3}\tau^4 + (\gamma_R a)^2(\frac{64}{3}\tau^2 + 16\tau^6) + (\gamma_R a)^4(\frac{64}{3} + \frac{16}{9}\tau^4)] +$$

$$+ \frac{(1+\beta k)^4}{(1-\beta k)^2}[\frac{3}{4}\tau^4 + (\gamma_R a)^2(3\tau^2 + \frac{5(1+\beta k)^2}{16(1-\beta k)^2}\tau^6) +$$

$$+ (\gamma_R a)^4(3 + \frac{5(1+\beta k)}{9(1-\beta k)^2}\tau^4)]\} + O((\gamma_R a)^6), \ \gamma_R a \to 0 \qquad (47)$$

In the special case $r_0 \to \infty$ $(\tau \to 0)$, by the relations (46), (47) we obtain [2],

$$\sigma = (\pi a^2)\{\frac{(1+\beta k)^2}{3} + \frac{3(1-\beta k)^4}{(1+\beta k)^2}\}(\gamma_L a)^4 + O((\gamma_L a)^6), \ \gamma_L a \to 0 \qquad (48)$$

or

$$\sigma = (\pi a^2)\{\frac{(1-\beta k)^2}{3} + \frac{3(1+\beta k)^4}{(1-\beta k)^2}\}(\gamma_R a)^4 + O((\gamma_R a)^6),\ \gamma_R a \to 0 \tag{49}$$

likewise in the case $\gamma_L a \to 0$ and $\gamma_R a \to 0$, by the relations (46), (47) we obtain [2],

$$\sigma^{sc}_{A,r_0} = \frac{1}{4} f_A(\beta, k)(\pi a^2)(a/r_0)^4 \tag{50}$$

where $A = L, R$, with $f_A(\beta, k) = \frac{(1-\varpi_A \beta k)^2}{3} + \frac{3(1+\varpi_A \beta k)^4}{(1-\varpi_A \beta k)^2}$ (51)

Choose a Cartesian coordinate system Oxψz, and five point-source locations, namely (0,0,0), (l,0,0), (0,l,0) (0,0,l) and (0,0,2l), which are at (unknown) distances r_0, r_1, r_2, r_3 and r_4, respectively from the sphere's center. The parameter l is a chosen fixed length. For each location, measure the leading order term in the low-frequency expansion of the scattering cross-section.

Thus, our five measurements are [2],

$$m_j = \frac{1}{4} f_A(\beta, k)\pi a^2 (\frac{a}{r_j})^4 \tag{52}$$
$$j = 0, 1, 2, 3, 4$$

Dimensionless quantities related to m_j are

$$\gamma_j = \frac{l}{\sqrt{m_j}} = 2\sqrt{\frac{1}{f_A(\beta, k)\pi}}\ \frac{l}{a}\ (\frac{r_j}{a})^2 \tag{53}$$
$$j = 0, 1, 2, 3, 4$$

equivalently, we obtain [2],

$$r_j^2 = \frac{1}{2}\sqrt{f_A(\beta, k)\pi}\ \frac{a^3}{l}\ \gamma_j \tag{54}$$
$$j = 0, 1, 2, 3, 4$$

There are six unknowns namely r_0, r_1, r_2, r_3, r_4 and a. Furthermore, r_0, r_3 and r_4 are related using the cosine rule, $r_4^2 + r_0^2 = 2r_3^2 + 2l^2$. So, we can find the six unknowns. The center of the spherical scatterer is obtained from the intersection of the four spheres centers at (0,0,0) (l,0,0), (0,l,0) and (0,0,l), with corresponding radius r_0, r_1, r_2, r_3 respectively.

References

[1] Athanasiadis C., Berketis N., "Scattering relations for point – source excitation in chiral media", Mathematical Methods in the Applied Sciences, Vol. 29, 2006, pp. 27-48

[2] Berketis M. Nikolaos, "Scattering spherical Electromagnetic waves in chiral media", PhD thesis, University of Athens – Department of Mathematics, December 2007

[3] Arnaoudov Y, Dassios G, Hadjinicolaou M., "The resistive coated sphere in the presence of a point generated wave field", Mathematical Methods in the Applied Sciences, Vol. 22, 1999, pp. 73-90

[4] Lakhtakia A., "Beltrami Fields in Chiral Media", World Scientific, Singapore, 1994, §2-1.3 (pp. 42-44), §2-2.3 (pp. 49-52), §4-1 (p. 130 Chapter 4), §5-1 (p. 164 Chapter 5), §6-1.1 (pp. 214-397), §8-2.1 (pp. 391-397), §9-2.3 (pp. 468- 473).

[5] Lakhtakia A, Varadan V.K., Varadan V.V., "Time-Harmonic Electromagnetic Fields in Chiral Media", Lecture Notes in Physics, Vol. 335, Springer, Berlin, 1989, §3-§4-§7-§11-§12-§13

[6] Athanasiadis C., "On the far field patterns for electromagnetic scattering by a chiral obstacle in a chiral environment", Journal of Mathematical Analysis and Applications, Vol. 309, 2005, pp. 517-533

[7] Morse P.M, Feshbach H., "Methods of Theoretical Physics, Part II", Mc Graw-Hill, 1953, pp. 1864-1866, 1870, 1871, 1887

Preprint Versions

"Direct and inverse scattering problems for spherical Electromagnetic waves in chiral media"
Christodoulos Athanasiadis and Nikolaos Berketis
"http://arxiv.org/abs/0812.2169"

*** About the Author**

Nikolaos Berketis, was born in Athens, Greece, 1952. Mathematics degree, Aristotle University of Thessaloniki, 1976. MSc in Applied Mathematics-Numerical Functional Analysis, Department of Mathematics, National and Kapodistrian University of Athens (UoA), 2003. Ph.D. in Applied Mathematics, Department of Mathematics, UoA, 2007. Professor of Secondary Education, 1980-2006. High school Principal, 2007-2012. Teacher at the UoA: Department of Informatics and Telecommunications, 2002-2003. Postgraduate program of the Department of Geology and Paleontology, 2003-2004. Research experience: Participation in the following research projects: 1) "The far-field operator in solving inverse scattering problem". Special Research Account 70/4/6412, UoA, 2002. 2) "Scattering of spherical electromagnetic waves by chiral materials". Special Research Account 70/4/6412, UoA, 2004. 3) "Mathematical analysis of wave propagation in chiral electromagnetic and elastic media." Pythagoras II: Reinforcing of University research groups (EPEAEK II), Department of Mathematics, UoA, 2005. Member of the Question Bank department of Evaluation and Training Research Center, Hellenic Mathematical Society (HMS), 2001-2004. Editorial Board experience: Member of the Scientific Committee of Euclid C΄ journal, Hellenic Mathematical Society (HMS). Member of the Scientific Committee of the project "Digital Training Textbooks for Pan-Hellenic examinations" -for Mathematics, Science and Technology Educational Path, 3rd grade, High School and Mathematics & Elementary Statistics, General Education, 3rd grade, High School- implemented by Computer Technology Institute University of Patra, for the Ministry of Education. Eighteen published peer-reviewed papers, more than 150 references, in peer-reviewed journals, utilizing both Hellenic and international bibliography. Participation in the project: "Change of speed of pulse wave after surgical narrowing of the descending thoracic aorta, "1st prize, Best Project award, 28th Annual Pan-Hellenic Medical Conference in the field of basic research, oral presentation, Athens, May 21-25, 2002. Personal work on the scattering of spherical electromagnetic waves in chiral media is posted at "The Smithsonian/NASA Astrophysics Data System" website. Authoring experience: Scientific research articles and books.

nberketis@gmail.com

Experimental Results on the Behavior of Water Droplets on Polymeric Surfaces Under the Influence of Electric Fields: the Case of an Inclined Test Arrangement for PVC, Rubber and Silicone Rubber

M.G. Danikas, P. Ramnalis, R. Sarathi *

Department of Electrical and Computer Engineering,
Democritus University of Thrace, Xanthi, Greece [1, 2]
Department of Electrical Engineering,
IIT Madras, Chennai- 600 036, India [3]

Abstract

This paper investigates the influence of various parameters on the behavior of water droplets on polymeric surfaces under electric fields. An inclined plane test was carried out to understand the droplet behavior in strong electric field. Parameters such as, water droplet conductivity, droplet volume, polymeric surface roughness and droplet positioning with respect to the electrodes were studied. The flashover voltage is affected by all aforementioned parameters. The droplet positioning is in some cases more vital than the droplet volume.

Introduction

Water droplets on a polymeric surface may cause corona under the influence of an electric field and can cause deterioration to insulation surface even in conditions of low pollution level. Water droplets on a polymeric surface increase locally the applied electric field. Local field intensifications lead to partial discharges (PD) and/or localized arcs, which may render possible the dry bands on the polymeric surface. Local arcing will eventually bridge the dry bands and a complete flashover will finally ensue. This mechanism is valid to a greater or lesser extent for both outdoor and indoor insulation, although each of the aforementioned categories have their own particular characteristics, namely that indoor insulation is stressed more and is subjected to a different type of environmental influences than outdoor insulation [1], [2]. A combination

of water droplets and dust-like impurities on the surface of a polymeric surface may lead to a conducting contamination layer, which may cause a reduction of the flashover voltage. The design of high voltage insulators, they can be for indoor or outdoor use, one should take into account not only the pollution level, the insulator material and the appropriate voltage level, but also the influence of water droplets on the flashover voltage. Previous work, carried out in this laboratory, tackled the behavior of water droplets for a wide range of water conductivities (1.7 μS/cm – 10000 μS/cm) [3], [4]. In both publications, it was shown that, among the factors influencing the behavior of the water droplets, were the water conductivity, polymer surface roughness, droplet volume and droplet positioning with respect to the electrodes.

In the present work, a study of the aforementioned parameters on the water droplet behavior under the influence of a uniform electric field in the range of 1.7 μS/cm – 2000 μS/cm was carried out. All tests were performed with an inclined test arrangement, in order to simulate the behavior of water droplets on the surface of a real insulator. The angle used with respect to the horizontal was 10°. Such an angle was chosen because of its immediate relevance to industrial insulators.

Force balance at the droplet/ polymer surface interface

A modeling of a wet contaminated surface was given in other publications and only a brief outline is provided here [5]. Condensation of droplets on the surface of a high voltage insulator can come about from droplet germs. In Fig. 1, the forces exercised on the droplet are shown in case where no electrical field is applied. Such forces are the surface tension of the liquid (τ_L), the surface tension of the solid (τ_S) and the interfacial tension between liquid and solid (δ_{SL}). When an electric field is applied, the droplet deforms because of an additional force. The tangential electric field on the surface of the insulator creates a force on the surface of the droplet which causes its deformation. The deformation of the droplet affects the field distribution. Local field intensifications may result, which will cause micro-discharges between the droplets. This is the beginning of the chemical deterioration of the insulator surface.

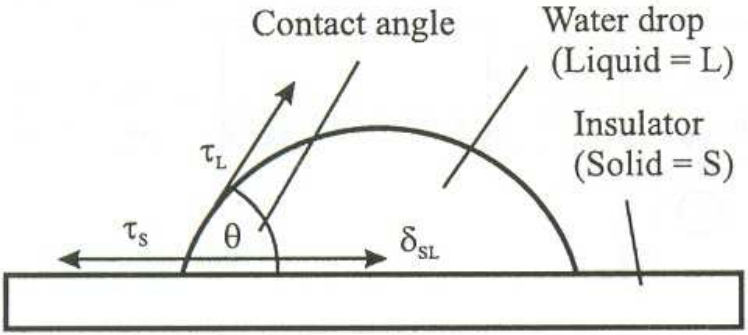

Fig. 1: Force balance at the interface solid/liquid at a water droplet on an insulating Surface (after [5])

Hydrophobicity may locally be lost. The voltage difference across the droplet will be diminished and micro-discharges will follow. Solvable nitrates, which are the result of the electrochemical deterioration, cause a higher conductivity of the water droplets. Dry zones may follow. It is important to bear in mind that not only the influence of the applied electric field on the shape of the droplet is of great significance, but also the influence of the disintegrated droplet on the electric field distribution [5], [6].

Hydrophobic polymeric surfaces are characterized by a low surface conductivity which in turn gives a low discharge activity and a higher flashover voltage. This holds also for polluted environments. Reduced hydrophobicity implies a higher risk for flashover of the insulator. Hydrophilic materials, on the other hand, are very sensitive to polluted environments, and are characterized by a significant activity of local discharges [7]. It is well known the classification of the Swedish Transmission Research Institute (STRI) regarding the hydrophobic and hydrophilic surfaces. STRI classifies the various surfaces according to their hydrophobicity from class 1 (most hydrophobic, with only discrete droplets on the surface with contact angle larger than 80°) to class 7 (most hydrophilic, with continuous water films forming on the surface). However, the truth is that no matter if the insulator has some sort of humidity and it is only slightly polluted or

it is heavily polluted, in both cases surface discharges play a most important role, and such discharges may start from water droplets.

Experimental arrangement and preparation of the samples

The aim of this paper is to study the behavior of water droplets under the influence of an electric field. The voltage supplied was from a 20 kV transformer (in practice the transformer may deliver voltages up to 1.2 times of its nominal voltage without loss of the accuracy of the measurement. Consequently, the applied voltages were accurate up to 24 kV). The electrodes used were of copper. A top view as well as a cross section of an electrode is shown in Fig. 2. The electrodes were half cylindrical in shape. Attention was paid to the smoothness of the electrode surfaces, so that no unnecessary field enhancements could be noticed.

The water droplets were positioned on the polymeric material surface with the aid of a special arrangement consisting of a metallic frame and three rules, one of which had two laser indicators. The water droplets were put on the surface with a syringe. Detailed information on the way the droplets were positioned on the polymeric surface is given in [3]. The photograph of the inclined plane test is shown in Fig. 3.

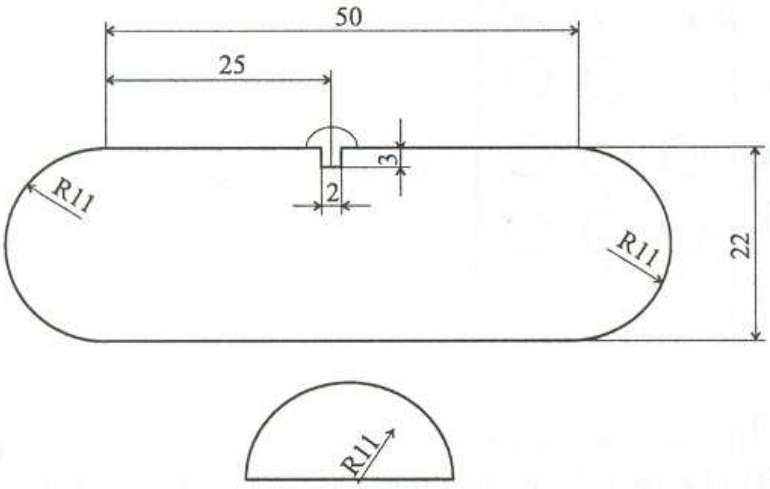

Fig. 2: Top view (above) and cross section (bottom) of the electrodes used (all dimensions in mm)

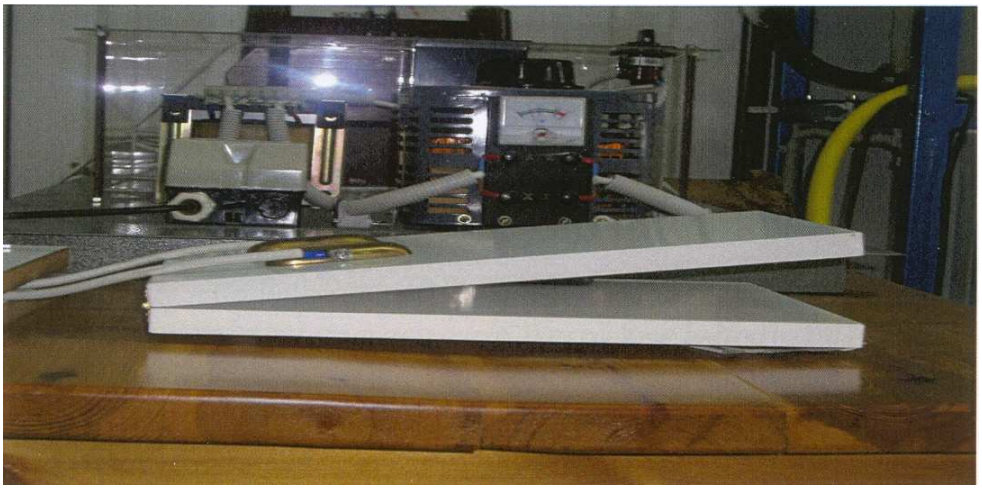

Fig. 3: The inclined Plane test setup (side view)

The polymeric materials used were PVC, rubber and silicone rubber. Surface roughness and resistivity of the material were measured. Surface roughness were measured using perthometer (Type Perthometer M4P). They gave a roughness of 0.25 µm for PVC, 0.79 µm for silicone rubber and 1.10 µm for rubber. Resistivity of the material were performed with a Megger (BM25 type) and they gave a resistivity of 206 GΩ for PVC, a resistivity of 3100 GΩ silicone rubber and a resistivity of 2660 GΩ for rubber. The above values of surface roughness and surface resistivity were not isolated values, but each of them was the mean of three measurements [8], [9].

In the present work, by mixing known quantity of NaCl in distilled water forming solutions with conductivity in the range 1.7 µS/cm to 2000 µS/cm, were used as droplet. The range of conductivity were chosen based on the conductivity of natural rain and its values lie in the range 50 - 150 µS/cm, whereas the tests with porcelain and glass insulators are performed with conductivities of 2500 µS/cm [10].

Experimental procedure

The materials used were PVC, silicone rubber and rubber. Various droplet arrangements were studied. These arrangements are given in Fig. 4. Each droplet had a volume of 0.2 ml. The electrodes were positioned at a distance of 4 cm from each other.

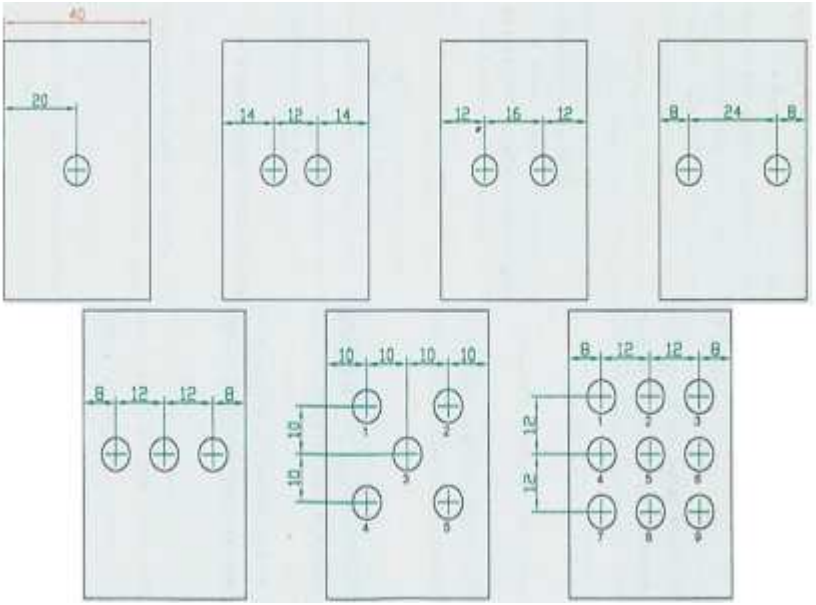

Fig. 4: Top view showing the droplet arrangements. Starting from top left, the arrangements were named as
(1) arrangement with 1 droplet,
(2a) arrangement with 2 droplets, 14-12-14,
(2b) arrangement with 2 droplets,12-16-12,
(2c) arrangement with 2 droplets, 8-24-8,
(3) arrangement with 3 droplets,
(5) arrangement with 5 droplets and
(9) arrangement with 9 droplets
All dimensions given are in mm and they symbolize the distances of the droplets from the respective electrodes and the distances between them

The parameters investigated were the water conductivity, the roughness of the insulating surface, the positioning of the droplets and their volume. The insulating surfaces were used as they were received from the manufacturer without any further treatment. After putting the droplets on the polymeric surface, the voltage was slowly raised until flashover occurred. After that and after cleaning the surface and putting new droplets on it, the voltage was raised again up to the previous flashover value minus 1.2 kV, so that no new flashover would occur.

At this voltage the arrangement would stay for 1 min. If no flashover occurred, the voltage was raised by 0.4 kV and the procedure was repeated until flashover occurred. The reason we left every time the voltage on for 1 min, was in order to give necessary time interval for the droplet(s) to deform and for the partial discharge to initiate.

It should be noted that it is observed a tendency for the droplets to slide, especially for PVC because of its smooth surface. The droplet slide was minimal in the case of rubber, which was the rougher of the three materials used. An elongation of the droplets was observed, as the applied voltage was larger. A more evident oscillation of the droplet was observed with silicone rubber. The reason for that was because the aforementioned material is more hydrophobic than the other two. Consequently, the droplet, for a defined droplet volume, has a smaller contact area with silicone rubber, and for this reason it oscillates more [8]. In some cases, such as with PVC with a droplet conductivity of 1.7 μS/cm and with the arrangement (1) of Fig. 4, ejection of minute charged droplets was observed just before flashover [11].

Experimental results

At first, experiments were performed without any droplets between the electrodes. This was done in order to have reference values of the flashover voltage and also to understand influence of number of droplets between the electrodes that would result in a reduction of the flashover voltage. The flash-over voltages without any droplets measured were 23 kV (± 0.5) for PVC, 25 kV (± 0.5) for silicone rubber and 24 kV (± 0.5) for rubber. The flash-over voltages of the three materials used were very similar.

In Figs. 5 - 11 the variation of flashover voltage with respect to the droplet conductivity for different droplet arrangements is shown.

It is evident that silicone rubber presents a higher flashover voltage than the other two materials. It should be noted, however, that in the case of droplet arrangements (5) and (9) where rubber seems to be as good as silicone rubber. A possible explanation might be that in such a case, the droplets cover a significant part of the polymeric surface and hence they play an even more important role than the polymer itself. This in combination with the fact that

the rubber has a rougher surface compared to the other two materials, has as a result the lesser oscillation in the case of rubber.

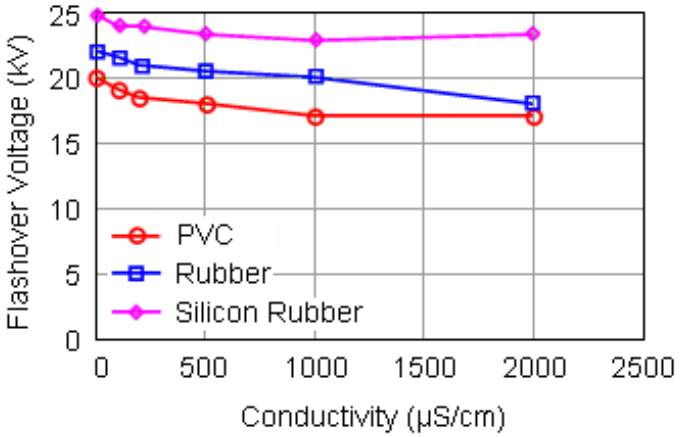

Fig. 5: Flashover voltage for droplet arrangement (1)

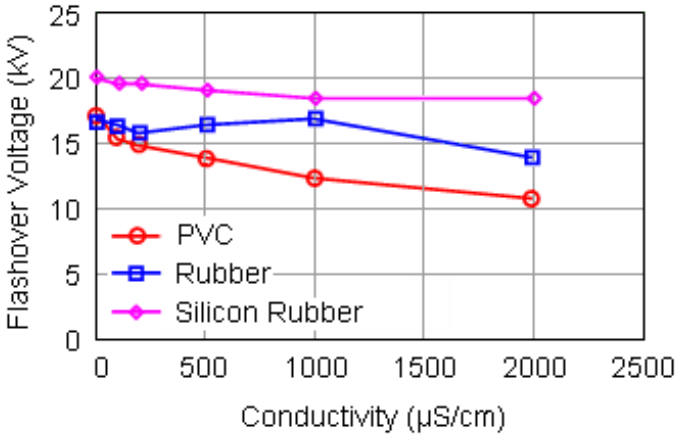

Fig. 6: Flashover voltage for droplet arrangement (2a)

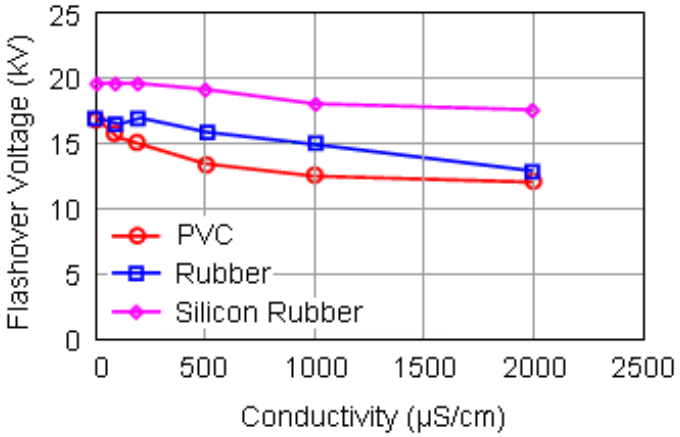

Fig. 7: Flashover voltage for droplet arrangement (2b)

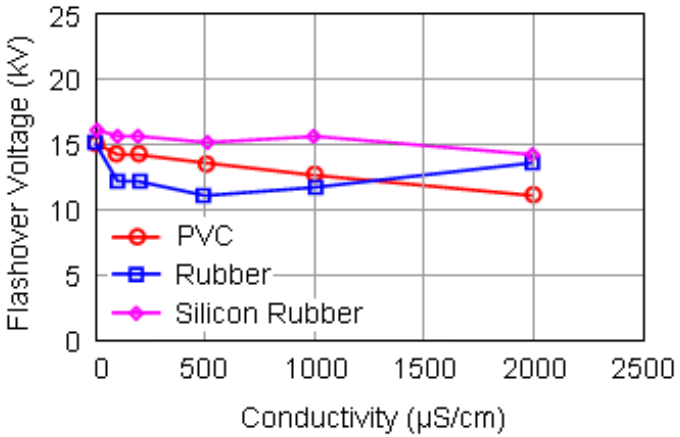

Fig. 8: Flashover voltage for droplet arrangement (2c)

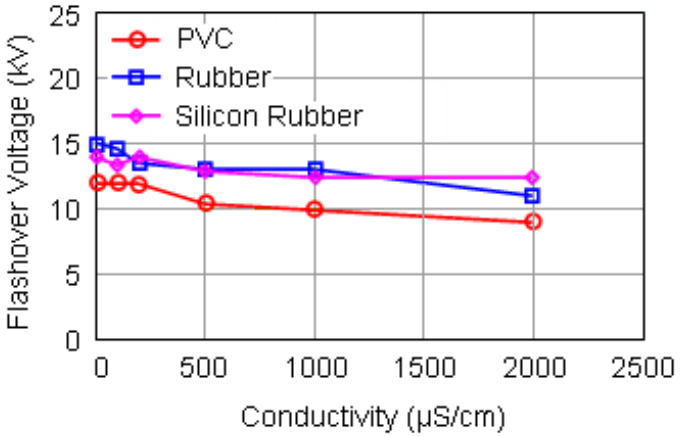

Fig. 9: Flashover voltage for droplet arrangement (3)

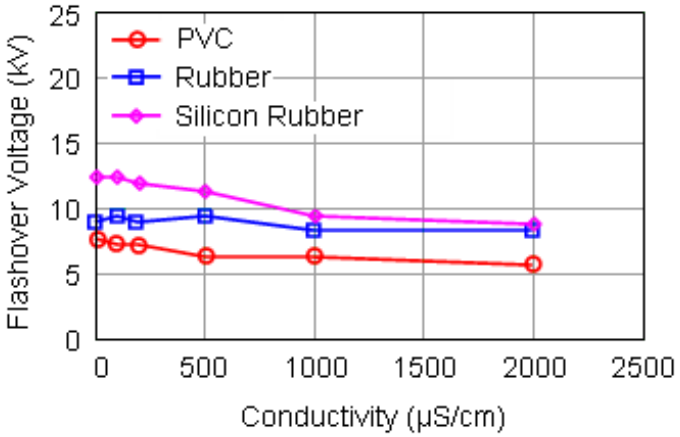

Fig. 10: Flashover voltage for droplet arrangement (5)

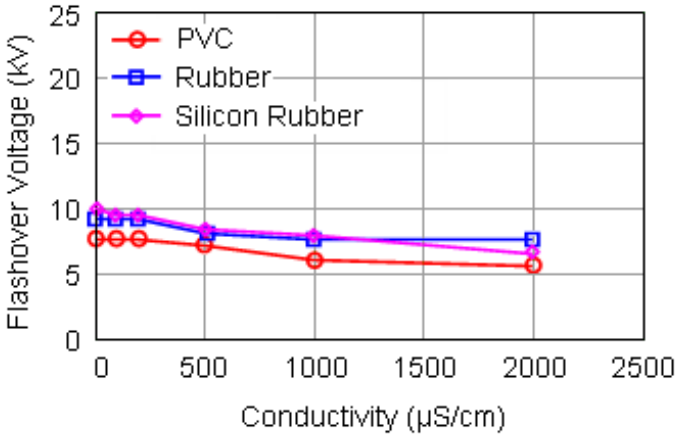

Fig. 11: Flashover voltage for droplet arrangement (9)

The better performance of silicone rubber is due to its hydrophobicity [5], [12]. The larger contact angle the droplets have minimum contact with the insulation material as in the case of silicone rubber. Figs. 12 - 14 show the influence of droplet volume on the flashover voltage. It is clear that the number of droplets affects the flashover voltage, i.e. the larger the number, the lesser the flashover voltage. An exception to that we have with the arrangement of 3 and 5 droplets. It is evident that larger flashover voltages were observed with 5 droplets than with 3 droplets. A possible explanation of that is that in the case of 3 droplets, the distance between electrode and droplet is smaller than in the case of 5 droplets. Consequently, one might say that there are occasions where the positioning of the droplets with respect to the electrodes which plays a more vital role than the whole droplet volume. A further validation of the above consists of the comparison of the flashover voltages in the cases of 3 and 9 droplets. It is observed that the flashover voltages for both these arrangements are not that different although the droplet volume triples.

An interesting case consists also of the droplets arrangements 2a, 2b and 2c. Higher values for flashover voltage were observed for arrangement 2a, then for arrangement 2b and the lower flashover voltage was observed for droplet arrangement 2c. This fact reinforces the above observations, namely that the positioning of the droplets play a crucial role, i.e. the closer the droplets to the electrodes, the lower the flashover voltage. It is to be noted that similar observations were made also in [3], [4], where not an inclined arrangement was used but a horizontal one. What is presented in this paper is an approach of the behavior of water droplets on polymeric surfaces with an inclined electrode arrangement. The results were reproducible but not that many tests were carried out which would allow a statistical study of the collected data. The main interest of this paper concentrates on the study of the behavior of the droplets. In the present context, no emphasis was given to the quantification of the studied parameters.

A comment should be made on the results with the conductivity of 1.7 μS/cm: in such a case, with such a low conductivity, the water path behaves like a load, i.e. like a resistance connecting the two electrodes. It is for this reason that we observed a lowering of the voltage at the output of the power source. The flow of current through water of low conductivity (i.e. of large resistance) means practically an increase of water temperature because of the power loss in the resistance of the water path. From the relation $P = I^2R$, we can conclude that as the resistance is larger, as in our case the water path of very low conductivity, the power loss at this resistance is larger. Consequently, the temperature developed in such a resistance is enough for the boiling of the water. A quantity of water evaporates and the water path becomes narrower. Dry zones are formed, micro-discharges ensue and finally the flashover follows. Such a phenomenon was observed in the inclined arrangement experiments, as they were observed before with non-inclined test arrangements [8].

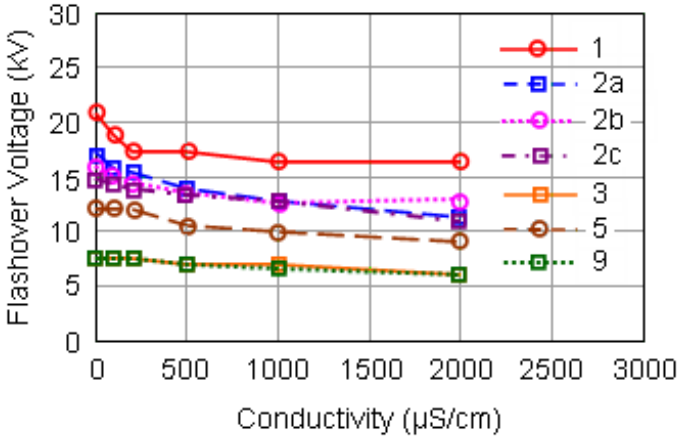

Fig. 12: Flashover voltage for various conductivities, positioning and volume of the droplets. PVC used

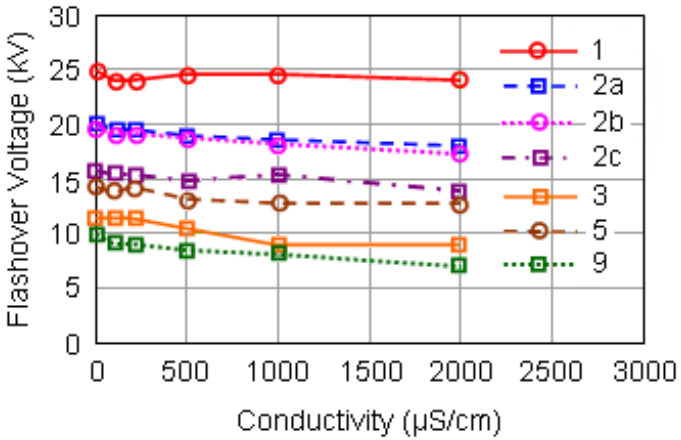

Fig. 13: Flashover voltage for various conductivities, positioning and volume of the droplets. Silicone rubber used

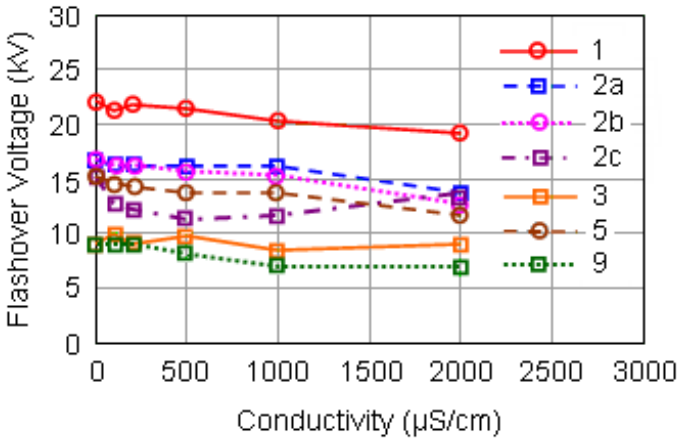

Fig. 14: Flashover voltage for various conductivities, positioning and volume of the droplets. Rubber used

Discussion and thoughts for further research

In the present paper, some parameters influencing the droplet behavior on polymeric surfaces were investigated, such as water conductivity, droplet volume, polymeric surface roughness and droplet positioning. An increase of conductivity causes a decrease of flashover voltage. This is a statement valid irrespective of the polymer used. The surface roughness affects in a positive way the flashover voltage, when the number of droplets is large. The surface roughness functions as a hindrance to the movement of the droplets, and consequently renders their oscillation more difficult. An increase of droplet volume causes a decrease of flashover voltage. This is in agreement with experimental observations published before with either ac or dc electric fields [13]. The position of the droplets with respect to the electrodes is of vital importance. With the droplets nearer the electrodes, the flashover voltage decreases. This is a phenomenon observed, albeit in different circumstances and conditions, also with enclosed cavities in solid dielectrics, where discharges become much more intense when one of the enclosing walls is an electrode [14].

The above show clearly that the polymeric material

plays a predominant role in determining the flashover voltage and the behavior of water droplets. Hydrophobic materials, such as silicone rubber, perform better than PVC or rubber. With this in mind, one should also note that most polymeric materials for outdoor applications present some sort of hydrophobicity. However, the advantage of silicone rubber consists in the fact that it does not only have this property, it can also regenerate it [15].

The formation of water paths, between the droplets as well as between the droplets and the electrodes, generally follow the direction of the applied electric field. The general activity in the form of discharges and droplet movement with rougher surfaces, sets in at higher voltages. In the case of just one droplet, with the application of the field, a deformation starts turning later to instability. Such behavior was observed with the inclined arrangement as well as with previous horizontal arrangements [3], [4]. Also in the case of the inclined arrangement, the role of the 'triple points' (i.e. the points where air, polymeric surface and droplet meet each other) is vital. The forces exercised on the droplets, because of the applied electric field, are quite strong, and therefore, the 'triple points' move towards the electrodes. Experimental data published recently, validate what is reported here [16]. Such movement of 'triple points' causes the spread of the droplets. The spread of droplets is perhaps the most characteristic phenomenon observed with the inclined electrode arrangement. It is not, however, the only one observed. Droplet oscillation, formation of water paths, collapsing of two droplets into a larger one, ejection of small charged droplets from a larger one, were also noted during the experiments. In this respect, the present work offers similar conclusions with those in [3], [4], [8], [9], [16], [17]. The importance of the triple points should be emphasized. In other works, it has been reported that partial discharge (PD) activity is sometimes marginal, not easily detectable by a conventional electrical PD system but by a photomultiplier. Smaller water droplets offer higher flashover voltages. This can also be explained by considering – in the case of smaller droplets – that the intermolecular forces are in equilibrium with the surface tension and, consequently, the electrical forces required to

disturb the equilibrium are higher. On the other hand, for larger droplets, the inner forces may be lower and, if the surface tension stays the same, the equilibrium can more easily be disturbed. In such a case, the PD activity will start earlier and at lower voltages, and therefore, the flashover voltage will be lower [18]. The fact that the contact angle increases with the decrease of water droplet volume, is something that cannot be underestimated [18]. Generally speaking, although the observations of [18] refer to silicone rubber samples only, the relevant conclusions are not different from the ones presented in this paper.

It is to be noted that the inclined electrode arrangement, used here, should not be compared by any means with the well known arrangement of the inclined plane test [19]. In the latter, a film of electrolyte is arranged to trickle down the back surface of a sheet and the samples are rated in terms of the voltage which causes a track to form in one hour [20]. In other words, the inclined plane test is a means of evaluating resistance to tracking and erosion of insulating materials for outdoor use, whereas the inclined electrode arrangement used in this work is a setup to study some parameters affecting the droplet movement on polymeric materials. The inclined plane test is an accelerating test [19]. The angle which was used in our experiments, i.e. the angle of 10°, was taken from real insulators. The purpose was to see the droplet behavior under an electric field in, as much as possible, real conditions. The present work confirms some general tendencies noted in [3], [4].

It would be interesting to try experiments, in which the contact angle will be accurately measured for both smaller and larger water droplets w.r.t. time. The purpose would be to see whether the contact angle diminishes with the passing of time and which diminution is more dramatic, that of the contact angle of smaller droplets or that of the contact angle of the larger droplets. Recent research indicated that the contact angle of droplets decreases with time, without, however, precising whether the rate of decrease is larger for smaller or for larger droplets [21]. Moreover, as noted before, an interesting point can be to study different modes of droplet deformation in terms of the four parameters investigated in this pa-

per [18], [22].

One last point should be raised: the research mentioned above was carried out with conventional polymers. It is remarkable that, most of the aforementioned points, i.e. the importance of the positioning of the droplets, the significance of the droplet volume and/or of the droplet number as well as the importance of the water conductivity, are points which are also important for non-conventional polymers, i.e for nanocomposite polymers. Work done recently in this laboratory emphasizes that parameters such as those investigated here, are also significant for nanocomposite polymers. In fact, the nature of phenomena such as surface discharges or flashovers, must have a common underlying denominator for both conventional polymers and nanocomposite polymers. Future research must also be directed in order to find the common grounds for surface discharge phenomena in both conventional and nanocomposite polymers [23], [24].

Conclusion

Water droplet conductivity, polymer surface roughness, droplet volume and the positioning of droplets with respect to the electrodes constitute important parameters affecting the behavior of droplets under the influence of an electric field with an inclined plane electrode arrangement. Increased conductivity, smoother polymer surfaces and increased droplet volume cause a reduction of the flashover voltage. The droplet positioning with respect to the electrodes plays a vital role in reducing the flashover voltage and, on occasions, is more important than the droplet volume.

Appendix – Elementary modeling

As mentioned above, the behavior of a droplet was modeled in [25], where the electric field E_N developed at one edge of the droplet is given by

$$E_N = U\,h/[a(h-a)] \qquad (1)$$

where, U is the applied voltage, a is the droplet radius and h is the distance of the center of the droplet from one of the electrodes. The electric field E_M on the opposite edge of the droplet is given by

$$E_M = U\,h(L-h)/[a(L-h-a)] \qquad (2)$$

where, L is the distance between the electrodes and the other symbols as in Eq. (1). As a droplet is positioned in the middle of the electrodes, the ratio E_N/E_M is expected to

be unity, and this was what was exactly obtained with the above equations. Considering Eq. (1), as $h \rightarrow a$, E_N tends to infinity. This is what we observed in the context of this work, namely that the closer a droplet is in one of the electrodes, the larger the electric field is getting, and consequently the more deleterious the consequences are. The above simple modeling is due to [25]. It was elaborated in [26], albeit with a non-inclined test arrangement. It must be mentioned that phenomena of very similar nature were observed also with the inclined test arrangement.

Remark

Main aspects of this paper were published in M.G. Danikas, P. Ramnalis and R. Sarathi, "A study of the behavior of water droplets on polymeric surfaces under the influence of electric fields in an inclined test arrangement", Journal of Electrical Engineering, Vol. 60, No. 2, 2009, pp. 94-99. The present version, however, contains additional comments on some aspects of the investigated polymeric materials as well as on a possible relation of the observed phenomena in nanocomposite polymers.

References

[1] Kind D., Kaerner H., "High Voltage Insulation Technology", Braunschweig: Eds. Vieweg, 1985

[2] Danikas M.G., "Surface Phenomena on Resin-Type Insulators under Different Electrical and Non-electrical Stresses in the Early Stage of Ageing", Facta Universitatis, Vol. 13, 2000, pp. 335-352

[3] Karakoulidis K., Danikas M.G., Rakitzis P., "Deterioration Phenomena on Insulating Surfaces due to Water Droplets", Journal of Electrical Engineering, Vol. 56, 2005, pp. 169-175

[4] Danikas M.G., Rakitzis P., Karakoulidis K., "Study of Parameters Related to Deterioration Phenomena due to Water Droplets on Polymeric Surfaces", Journal of Electrical Engineering, Vol. 57, 2006, pp. 130-137

[5] Kloes H.J., Koenig D., Danikas M.G., "Electrical Surface Discharges on Wet Polymer Surfaces", Proceedings of the 8th International Symposium of Gaseous Dielectrics, Virginia beach, Virginia, USA, June 1998, pp. 489-495

[6] Koenig D., "Surface and Aging Phenomena on Organic Insulation under the Condition of Light Contamination and High Electric Stress", Proceedings of the Nordic Insulation Symposium, Vaasa, Finland, June 1994, pp. 17-35
[7] Hartings R., "The AC-Behavior of a Hydrophilic and Hydrophobic Post Insulator During Rain", IEEE Winter Power Meeting, New York, USA, 1994
[8] Karakoulidis K., "Breakdown Phenomena on Insulating Surfaces", M.Sc. Thesis, Democritus University of Thrace, Xanthi, Greece, 2002 (in Greek)
[9] Rakitzis P., "Flashover Phenomena on Polymeric Surfaces under the Influence of a Uniform Electric Field", M.Sc. Thesis, Democritus University of Thrace, Xanthi, Greece, 2003 (in Greek).
[10] Danikas M.G., "Ageing Properties of Silicone Rubber Materials Used in High Voltage Composite Insulators", Journal of Electrical and Electronics Engineering, Australia, Vol. 15, 1995, pp. 193-202
[11] Dan Windmar, "Water Droplet Initiated Discharges in Air", PhD Thesis, Uppsala, University, Uppsala, Sweden, 1994
[12] Gorur R.S., "High Voltage Outdoor Insulation Technology", Control and Dynamic Systems, Vol. 44, 1991, pp. 131-191
[13] Schutte, T., "Water Drop Dynamics and Flashover Mechanisms on Hydrophobic Surfaces", Proceedings of the Nordic Insulation Symposium, Vasteras, Sweden, paper 8.1, June, 1992
[14] Mason J.H., "Discharges", IEEE Transactions on Electrical Insulation, Vol. 13, 1978, pp. 211-238
[15] Vlastos A., Gubanski S., "Surface Structural Changes of Naturally Aged Silicone Rubber and EPDM Composite Insulators", IEEE Transactions on Power Delivery, Vol. 6, 1991, pp. 888-900
[16] Keim S.,Koenig D., Hinrichsen V., "Experimental Investigations on Electrohydrodynamic Phenomena at Single Droplets on Insulating Surfaces", Annual Report of the Conference on Electrical Insulation and Dielectric Phenomena, Albuquerque, New Mexico, USA, October 2003, pp. 133-136
[17] Keim S., "Optical Diagnostic of Single Droplets on Polymeric Insulating Surfaces in an Electric Field to Describe the Phenomena of the Beginning of Aging Mechanisms", PhD Thesis, Darmstadt University of Technology, Darmstadt, Germany, 2003 (in German).

[18] Feier-Iova S., "The Behaviour of Water Droplets on Insulating Surfaces Stressed by Electric Field", PhD Thesis, Darmstadt University of Technology, Darmstadt, Germany, 2009
[19] IEC 60 587 and BS 5604 Method of Test for Evaluating Resistance to Tracking and Erosion of Electrical Insulating Materials Used under Severe Ambient Conditions
[20] Stannett A.W., "Breakdown Testing and Measurements on Installed Equipment, In: Electrical Insulation", A. Bradwell (Ed.), London: Peter Peregrinus Ltd., 1983, pp. 261-276
[21] Fijii O., Honsali K., Mizuno Y., Naito K., "A Basic Study on the Effect of Voltage Stress on a Water Droplet an a Silicone Rubber Surface", IEEE Transactions on Dielectrics and Electrical Insulation, Vol. 16, 2009, pp. 116-122
[22] Fijii O., Honsali K., Mizuno Y., Naito K., "Vibration of a water Droplet on a Polymeric Insulating Material Subjected to AC Voltage Stress", IEEE Transactions on Dielectrics and Electrical Insulation, Vol. 17, 2010, pp. 566-571
[23] Kechagia S., Danikas M.G., Sarathi R., "Water Droplets and Breakdown Phenomena on Polymer Nanocomposite Surfaces under the Influence of Uniform Electric Fields", Malaysian Polymer Journal, Vol. 8, No. 2, 2013, pp. 41-47
[24] Bairaktari A., Danikas M.G., Zhao X., Cheng Y., Zhang Y., "Behaviour of Water Droplets under the Influence of a Uniform Electric Field in Nanocomposite Samples of Epoxy Resin/TiO_2", Engineering, Technology & Applied Science Research, Vol. 3, No. 5, 2013, pp. 511-515
[25] Imano A.M., Beroual A., "Deformation of Water Droplets on Solid Surface in Electric Field", Journal of Colloidal Interfacial Science, Vol. 298, 2006, pp. 869-879
[26] Cheng Y., Zhao X., Danikas M.G., Christantoni D., Zairis P., "A Study of the Behaviour of Water Droplets under the Influence of Uniform Electric Field in Epoxy Resin Samples, Journal of Electrical Engineering, Vol. 63, No. 3, 2012,pp. 196-200

*** About The Authors**

Michael Danikas, received the B.Sc. and M. Sc. from the University of Newcastle-upon-Tyne, England, in 1980 and 1982 respectively. He received the Ph.D. from the University of London, Queen Mary College, London, England, in 1985. He was employed at Eindhoven University of Technology, The Netherlands, and at ABB, Switzerland during the years 1987-1993. At present he is Professor at the Dept. of Electrical and Computer Engineering, Democritus University of Thrace, Xanthi, Greece. His research interests were and still are electrical trees in polymeric materials, the role of humidity on flashover voltage, transformer oil ageing and solid/liquid insulation ageing.
mdanikas@ee.duth.gr

Pavlos Ramnalis, graduated from the Dept. of Electrical and Computer Engineering, Democritus University of Thrace, in 2010. Afterwards he was employed in private companies in Athens, Greece.

Ramanujam Sarathi, is Professor at the Dept. of Electrical Engineering, Indian Institute of Technology Madras, Chennai, India. During his career, he spent a lot of time having worked with researchers at Akita University, Japan, and at Waseda University, Japan, on subjects such as properties of insulting materials, nanopowder technology and characterization of electrical trees in insulating structures.

[This Page Intentionally Left Blank]

Measurement Uncertainty in Network Analyzers: Differential Error Analysis of Error Models Part 3: Short One-Port Calibration – Comparison

N.I. Yannopoulou, P.E. Zimourtopoulos *

Antennas Research Group, Austria – Hellas [1, 2]
EECE Dept, Democritus University of Thrace, Hellas [2]

Abstract

In order to demonstrate the usefulness of the only one existing method for systematic error estimation in VNA (Vector Network Analyzer) measurements by using complex DERs (Differential Error Regions), we compare one-port VNA measurements after the two well-known calibration techniques: the quick reflection response, that uses only a single S (Short circuit) standard, and the time-consuming full one-port, that uses a triple of SLO standards (Short circuit, matching Load, Open circuit). For both calibration techniques, the comparison concerns: (a) a 3D geometric representation of the difference between VNA readings and measurements, and (b) a number of presentation figures for the DERs and their polar DEIs (Differential Error Intervals) of the reflection coefficient, as well as, the DERs and their rectangular DEIs of the corresponding input impedance. In this paper, we present the application of this method to an AUT (Antenna Under Test) selected to highlight the existence of practical cases in which the time consuming calibration technique results a systematic error estimation stripe including almost all of that of quick calibration.

Introduction

The systematic error in a full one-port calibrated VNA measurement ρ of a given one-port DUT (Device Under Test) is already estimated by its DER [1]-[2]:

$$\rho = (m - D)/[M(m - D) + R] \quad (1)$$

$$d\rho = [-RdD - (m - D)^2 dM - (m - D)dR + Rdm] / [M(m - D) + R]^2 \quad (2)$$

where m is the VNA complex reading and D, M and R are the complex system errors of Fig. 1.

The relations holding between this complex reflection

coefficient ρ and its respective impedance Z, as well as, between their DERs are [1]-[2]:

$$Z = Z_0(1 + \rho)/(1 - \rho) \quad (3)$$

$$dZ = 2Z_0 d\rho/(1 - \rho)^2 \quad (4)$$

In this paper, we express the DERs for systematic error estimation in VNA measurements calibrated by the much simpler and quicker reflection response technique, in order to be in place to make some practical decisions from the different calibration techniques comparison.

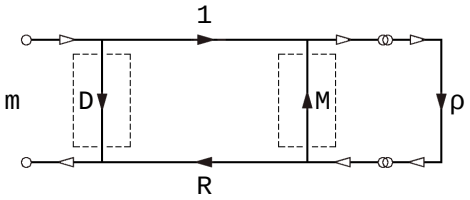

Fig. 1: Full one-port error model

Response Calibration

The reflection response calibration technique can be accomplished with the measurement of only one standard load, instead of three in full one-port, usually of a S short circuit [3]-[4]. This means that the flow graph of Fig. 1 is simplified a lot, since the two surrounded by dashed boxes system error branches of directivity D and source match M do not exist, equivalently D = 0 and M = 0 and (1) results to:

$$R = m/\rho_S = s/S \quad (5)$$

where s is the VNA complex reading of the *S* short circuit standard with a nominal value of S = – 1, m is the complex reading of a given DUT and ρ_S is its complex reflection coefficient as it is measured after this response calibration:

$$\rho_S = (m/s)S \quad (6)$$

which, from (2), has the differential error:

$$d\rho_S = (S/s)dm - (Sm/s^2)ds + (m/s)dS \quad (7)$$

The corresponding total DER is then the sum of L = 3 parallelograms. Therefore, this DER contour is a polygonal line with 4L = 12 line segments and vertices at most, in contrast with the DER of the measurement after a SLO full one-port calibration, which is a piecewise curve composed of 4(L – 1) = 24 line segments, 4(L – 1) = 24 circular arcs and 8(L – 1) = 48 vertices, at most [1]-[2].

Application Results

By following the error estimation process, we already detailed in [1]-[2], we take as dS the considered manufacturers' standard S uncertainty data:

$$-0.01 \le d|S| \le 0, \quad -2° \le d\angle S \le +2°$$

and as dm and ds the VNA inaccuracy of ±1 digit in LSD of their corresponding readings, for either the amplitude in decibels or the phase in degrees. Moreover, the one-port DUT that was considered is the same typical UHF ground-plane antenna (that is: AUT) mentioned in [1].

The difference between the 3 nominal values (–1, 0, 1) of the 3 full one-port calibration standards (S, L, O), respectively, and their 3 corresponding VNA readings (s, l, o), can be estimated by the extent of the surfaces shown in the triptych of Fig. 2, where the vertical axis segment represents the range of the distinct stepped frequencies. Each surface is formed by parallel to horizontal plane lines. Each such line expresses the complex difference between the standard nominal value and its corresponding VNA reading, in each stepped frequency.

In the triptych of Fig. 3, and from left to right we have the difference surfaces made by distance lines between:

(a) the measured reflection coefficient ρ after a full SLO one-port calibration (black solid points) and the corresponding VNA readings m for the AUT measurement (colored magenta points),

(b) the measured reflection coefficient ρ_s after S response calibration (black ring points) and the corresponding VNA readings m for the AUT measurement (colored magenta points), and

(c) the two measurements (ρ, ρ_s).

All the involved, previously shown, quantities are projected on the horizontal complex plane of Fig. 4. The magenta colored spiral represents m, while, the black curves the reflection coefficient: solid points, for ρ, and ring points for ρ_s. All of l VNA readings are close enough to complex origin (colored green points). It is rather difficult to distinguish the two curves for s and o VNA readings, which are close enough to the unit circle circumference (colored red solid points and colored blue ring point, respectively).

The ρ-DERs and ρ_s-DERs, for all 4 MHz stepped frequencies covering the range of [600, 1000] MHz, are overlapped on the complex plane of Fig. 5, forming a light and a dark gray stripes, respectively. From each stripe we selected 11 DERs out of 101, drawn with dark gray and white colors respectively, to illustrate their outline dependence on frequency.

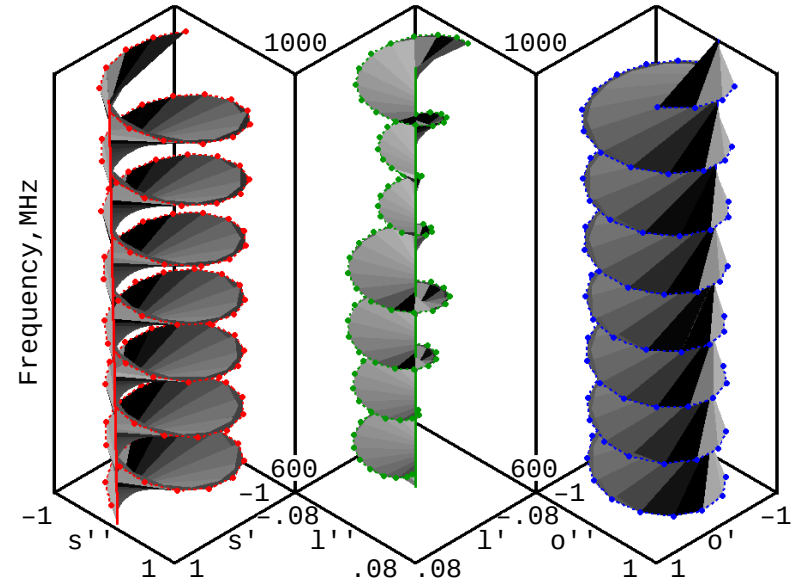

Fig. 2: Difference between s and S, l and L, o and O

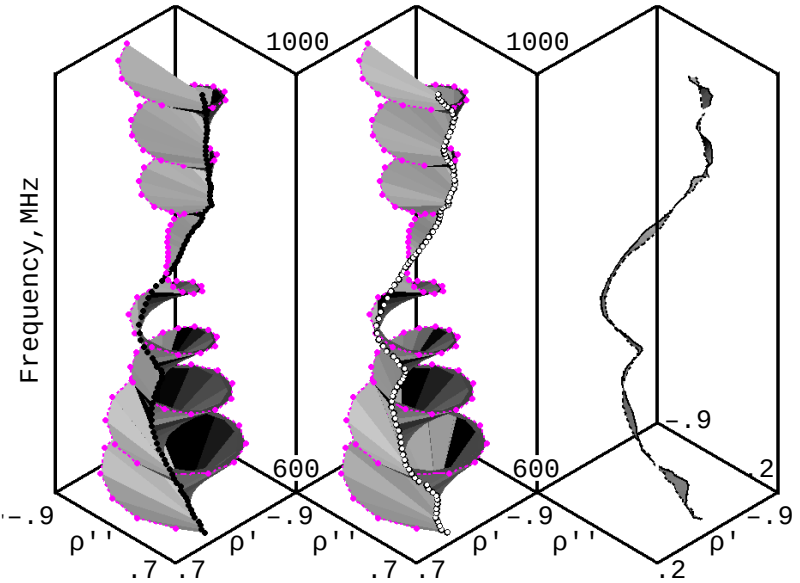

Fig. 3: Difference between m and ρ, m and ρ_S, ρ and ρ_S.

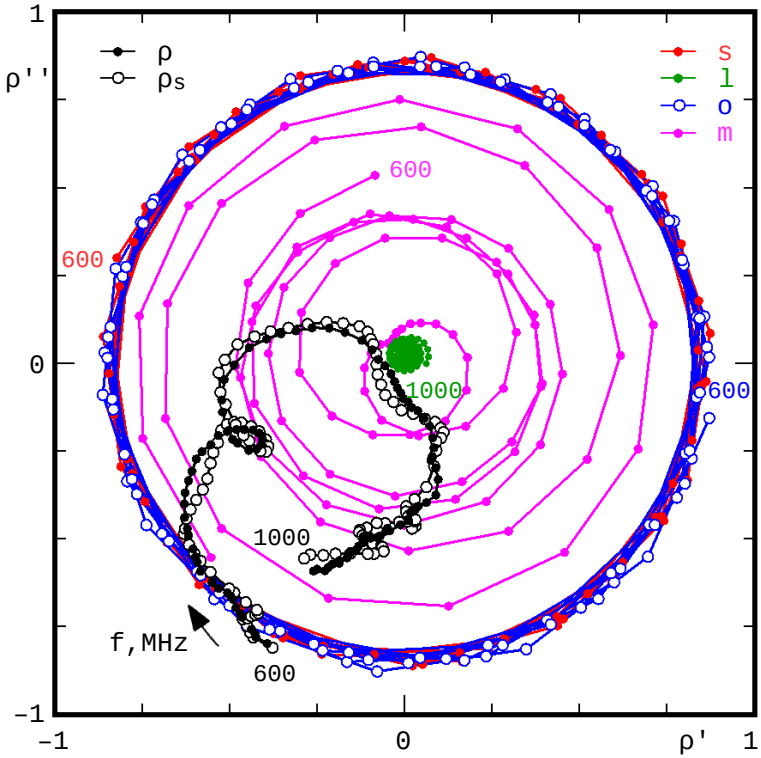

Fig. 4: VNA s, l, o, m readings and ρ, ρ_s measurements.

Moreover, we selected to magnify a part of this figure in the sub-range of [892, 1000] MHz, to further illustrate the DER outlines and their overlapping in Fig. 6, where the clearly shown ripple of the simple response calibration stripe over the relatively smooth full one-port calibration stripe reveals the superiority of the latter in the production of more accurate measurements.

The comparison between the AUT measurements based on these two calibration techniques is extended to the comparison against the frequency:

(a) of the computed polar DEIs of the reflection coefficient magnitude and argument stripes in Fig. 7,

(b) of the rectangular DEIs for the corresponding R input resistance and X input reactance stripes, in Fig. 8 and

(c) of the Z-DERs, and Z_s-DERs stripes in Fig. 9.

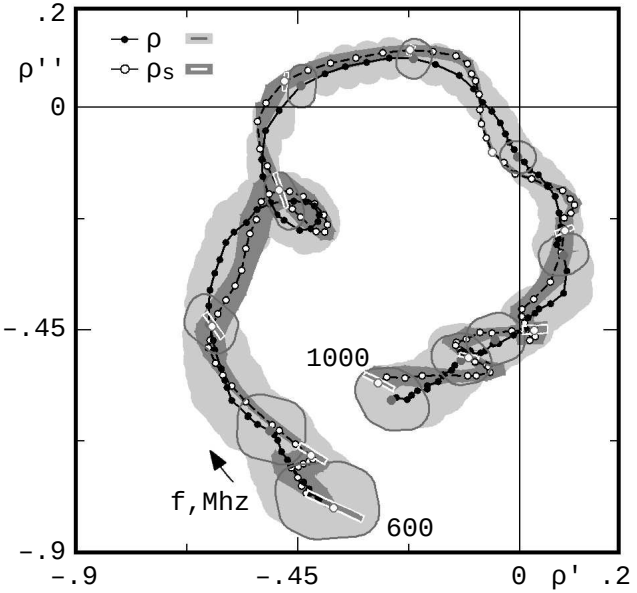

Fig. 5: Complex ρ-DERs and ρ_s-DERs in [600, 1000] MHz

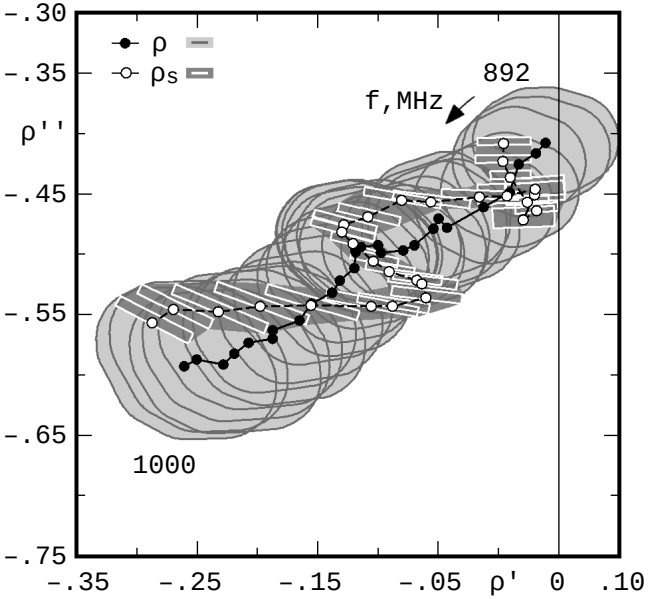

Fig. 6: Complex ρ-DERs and ρ_s-DERs in [892, 1000] MHz

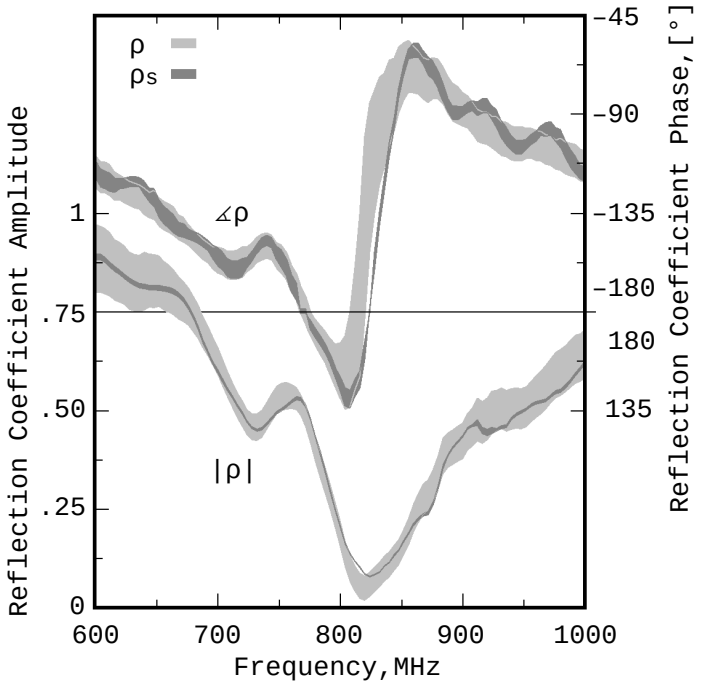

Fig. 7: Polar DEIs of reflection coefficient

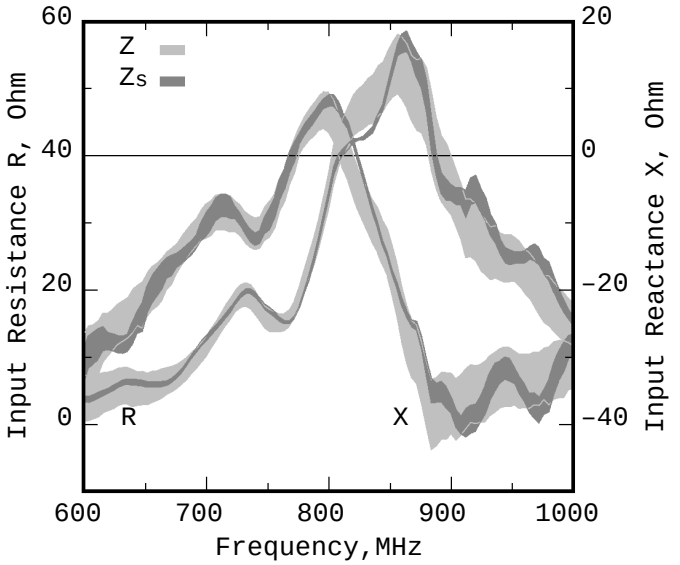

Fig. 8: Rectangular DEIs of input impedance

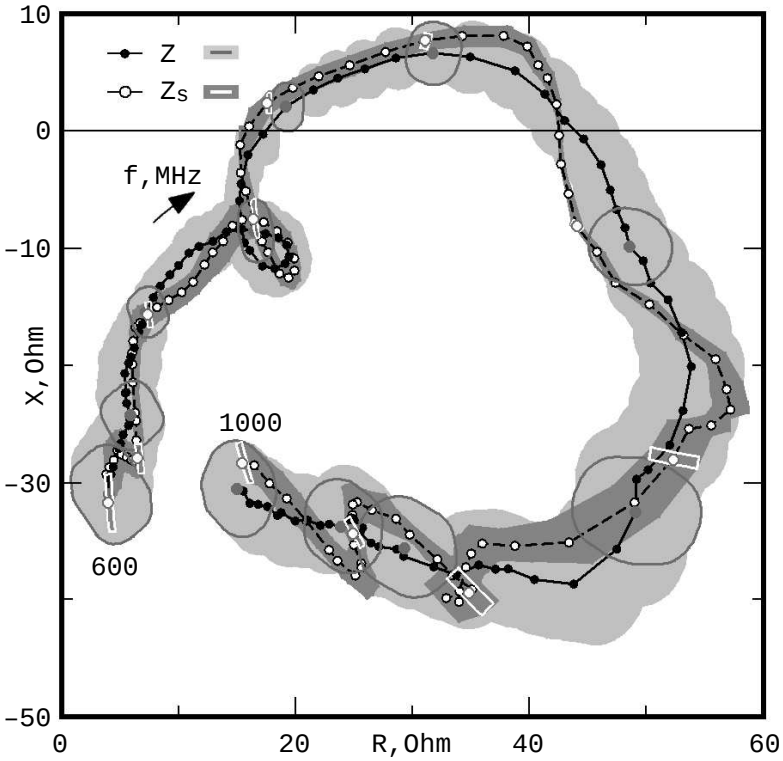

Fig. 9: Complex Z-DERs and Z_S-DERs in [600, 1000] MHz

Conclusion

From all that, it must be clear now that in this intentionally selected for presentation particular AUT case there was no advantage at all in selection of full one-port calibration over the reflection response one, due to their remarkable in all aspects coincidence. Of course this is just another one conclusion a-posteriori.

References *

[1] Yannopoulou N., Zimourtopoulos P., "Total Differential Errors in One Port Network Analyzer Measurements with Application to Antenna Impedance", Radioengineering, Vol. 16, No. 2, June 2007, pp. 1-8 "www.radioeng.cz/fulltexts/2007/07_02_01_08.pdf"

[2] Yannopoulou N.I., Zimourtopoulos P.E., "Measurement Uncertainty in Network Analyzers: Differential Error Analysis of Error Models Part 1: Full One-Port Calibration", FunkTechnikPlus # Journal, Issue 1, October 2013, pp. 17-22 "www.otoiser.org/index.php/ftpj/article/view/42"

[3] HP, "Vector Measurements of High Frequency Networks", Hewlett-Packard, 1989, pp. 2-13, 2-15, 3-11, 3-12

[4] AGILENT, "OPEN/SHORT Response Calibration (reflection test), Calibration Types and Characteristics" "http://ena.support.keysight.com/e5071c/manuals/webhelp/eng/measurement/calibration/calibration.htm"

*Active Links: 15.12.2013 - Inactive Links : FTP#J Link Updates: "http://updates.ftpj.otoiser.org/"

Preprint Versions

"Comparison of Error Estimation by DERs in One-Port S and SLO Calibrated VNA Measurements and Application"

Nikolitsa Yannopoulou, Petros Zimourtopoulos
"http://arxiv.org/abs/1102.4239"

Follow-Up Research Paper

Not until now

Previous Publication in FUNKTECHNIKPLUS # JOURNAL

"Measurement Uncertainty in Network Analyzers: Differential Error Analysis of Error Models Part 2: Full Two-Port Calibration", Issue 1, pp. 23-30

* About The Authors

Nikolitsa Yannopoulou, Issue 1, p. 15

Petros Zimourtopoulos, Issue 1, p. 15

[This Page Intentionally Left Blank]

[This Page Intentionally Left Blank]

FRONT COVER VIGNETTE

A faded synthesis of an anthemion rooted in a meandros

The thirteen-leaf is a symbol for a life tree leaf.
"Herakles and Kerberos", ca. 530–500 BC,
by Paseas, the Kerberos Painter,
Museum of Fine Arts, Boston.

www.mfa.org/collections/object/plate-153852

The simple meandros is a symbol for eternal immortality.
"Warrior with a phiale", ca. 480–460 BC,
by Berliner Maler,
Museo Archeologico Regionale "Antonio Salinas" di Palermo.

commons.wikimedia.org/wiki/File:Warrior_MAR_Palermo_NI2134.jpg